R-03-02

# Äspö Pillar Stability Experiment

# Summary of preparatory work and predictive modelling

J Christer Andersson
Svensk Kärnbränslehantering AB

November 2004

**Svensk Kärnbränslehantering AB**
Swedish Nuclear Fuel
and Waste Management Co
Box 5864
SE-102 40 Stockholm Sweden
Tel 08-459 84 00
+46 8 459 84 00
Fax 08-661 57 19
+46 8 661 57 19

ISSN 1402-3091
SKB Rapport R-03-02

# Äspö Pillar Stability Experiment

## Summary of preparatory work and predictive modelling

J Christer Andersson
Svensk Kärnbränslehantering AB

November 2004

*Keywords:* Pillar, Spalling, Numerical modelling, TASQ, In situ stress, Examine 3D, FRACOD, FLAC, JobFem.

# Abstract

The Äspö Pillar Stability Experiment, APSE, is a large scale rock mechanics experiment for research of the spalling process and the possibility for numerical modelling of it. The experiment can be summarized in three objectives:

- Demonstrate the current capability to predict spalling in a fractured rock mass.
- Demonstrate the effect of backfill (confining pressure) on the rock mass response.
- Comparison of 2D and 3D mechanical and thermal predicting capabilities.

This report is a summary of the works that has been performed in the experiment prior to the heating of the rock mass. The major activities that have been performed and are discussed herein are:

1) The geology of the experiment drift in general and the experiment volume in particular.
2) The design process of the experiment and thoughts behind some of the important decisions.
3) The monitoring programme and the supporting constructions for the instruments.
4) The numerical modelling, approaches taken and a summary of the predictions.

In the end of the report there is a comparison of the results from the different models. Included is also a comparison of the time needed for building, realizing and make changes in the different models.

# Sammanfattning

Äspö Pillar Stability Experiment, APSE är ett storskaligt bergmekanikförsök. Försöket skall studera spjälkning (spalling) i berg och undersöka vår möjlighet att numeriskt modellera initieringen av spjälkningsprocessen. Försöket har tre huvudmålsättningar:

- Demonstrera vår nuvarande förmåga att prediktera spjälkning i en något uppsprucken bergmassa.
- Demonstrera effekten av återfyllnad (mothållande tryck) på bergmassans respons.
- Jämföra mekaniska och termiska prediktioner gjorda med 2- och 3-Dimensionella modeller.

Denna rapport är en sammanfattning av det arbete som utförts inom experimentet fram till den tidpunkt då värmningen av bergmassan startade. De huvudsakliga delaktiviteterna har varit:

1) Dokumentering av geologin i experimentorten i allmänhet samt experimentområdets geologi i synnerhet.
2) Designen av experimentet samt tankarna bakom några av de viktiga besluten.
3) Framtagning av moneteringsprogrammet samt designen av stödkonstruktionen för de instrument som placerades i hålet.
4) Angreppssättet för den numeriska modelleringen samt en sammanfattning av gjorda prediktioner.

I slutet på rapporten är en jämförelse gjord på resultatet från de olika numeriska modelleringarna. Där finns även en jämförelse för den tid det tagit att bygga, realisera och göra ändringar i de olika modellerna.

# Contents

# 1 Introduction

At the Äspö Hard Rock Laboratory SKB has undertaken the rock mechanics experiment Äspö Pillar Stability Experiment, APSE. The experiment is a large scale test to investigate the spalling process and the effect of confining pressure on the spalling process. To induce stresses in the studied rock volume the in situ stresses will be concentrated by the choice of tunnel geometry and by the boring of two vertical boreholes of deposition hole size close to each other. The rock in the hole walls will then be highly stressed but not high enough to initiate spalling. To start the spalling process the stresses will be further increased by heating of the rock volume between the boreholes.

The effect of the confining pressure will be studied by applying a uniform pressure of 0.8 MPa to the wall of the first hole drilled. The pressure will be maintained during the drilling of the second hole and the heating phase of the experiment. The pressure will then be stepwise reduced and the rock mass response monitored via an acoustic emission system.

## 1.1 Background

During the construction of a future deep repository for spent nuclear fuel it is important that the geometry of the drifts, the spacing and the intersections between them are well designed. Since the repository will be located at great depth, 400–700 m, the in situ stresses may be quite high. If the design of the drifts concentrates the stresses at certain locations it is possible that brittle failure may occur in the form of spalling or in the worst case, minor rock bursts.

During the 100,000 years life time of the repository one of the design criteria is an ice load of approximately 3,000 m. It is possible that the enhancement of the in situ stresses due to this load may also initiate spalling in the deposition hole walls or the backfilled access drift despite the confining swelling pressure from the saturated bentonite buffer and backfill, if not properly designed.

To match the abovementioned design criterions enhanced knowledge of the failure mechanisms in granitic rock from the Scandinavian shield is necessary. At the Äspö HRL there are unique possibilities to study this process. Even though the experiment is carried out 450 m below the rock surface the rock mass response to the stress redistribution due to the excavations is essentially elastic /Andersson and Martin, 2003/. This makes it possible to follow the rock mass behaviour when it is loaded from an elastic response through the transitional zone defined by increased micro cracking into the final brittle failure phase. In Figure 1-1 the simplified graph of an ideal failure mode of a compressed core is presented. The three different axes represent stress, strain and the acoustic emission hit rate which is a measure of the micro cracking rate.

Even if we have good knowledge of the failure processes in the rock we need to be able to make accurate predictions. For this purpose there are a number of different numerical tools available. The accuracy of the predictions from the tools is unknown. An equally important part of the pillar stability experiment is therefore to use numerical models for predictions and compare the results to the actual outcome of the experiment.

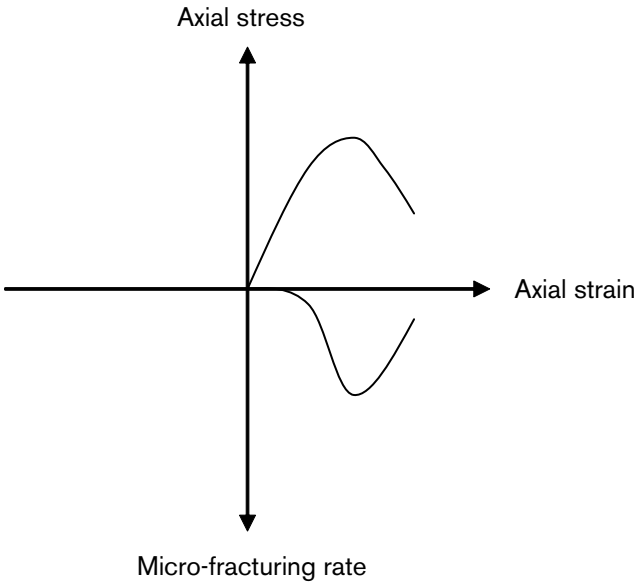


***Figure 1-1.*** *Ideal relationship between stress, strain and micro cracking rate in a compressed core.*

## 1.2 Objectives

The Äspö Pillar Stability Experiment has the following three main objectives:

1. Demonstrate the current capability to predict spalling in a fractured rock mass.
2. Demonstrate the effect of backfill (confining pressure) on the rock mass response.
3. Comparison of the mechanical and thermal predicting capabilities of 2D and 3D numerical models.

The experiment has hence been designed and planned to meet these objectives.

# 2 Geological overwiev

A comprehensive document of the geology and rock mechanics properties of the 450 m level of the Äspö HRL in general and the TASQ area in particular is presented in /Staub et al. 2004/. The characterization work described by Staub et al 2004 had two major objectives: 1) derive material properties for the final numerical modelling of the experiment, and 2) ensure that the pillar location is suitable from a structural and rock mechanical point of view. In summary the following activities have been performed:

- Geological mapping of the drift, the firs large hole bored (DQ0066G01) and the core boreholes.
- 3D-visualisation of the geological mapping in the experiment (pillar) volume of TASQ.
- Convergence measurements during the excavation and back calculation of the results for determination of the stress tensor and the rock mass Young's modulus.
- Laboratory tests on core samples from the 15 ∅76 mm core boreholes drilled around the pillar volume for determination of: compressive strength, thermal properties and fracture properties.
- P-wave velocity measurements on core samples and between boreholes for estimation of the excavation damaged zone and rock mass properties.

The properties in TASQ where found to be similar, with one exception, to what earlier has been assessed for the 450 m level. A heavily oxidized, brittle-ductile shear zone strikes along the TASQ-tunnel dipping to the southeast. The strength of the rock belonging to this zone is considerably lower than for fresh Äspö diorite depending on its brecciaed structure with weak fracture fillings.

The geological mapping has been digitalized, transformed to 3D-models. In Figure 2-1 and Figure 2-2 are resulting 3D-visualisations of the fractures in the TASQ tunnel presented.

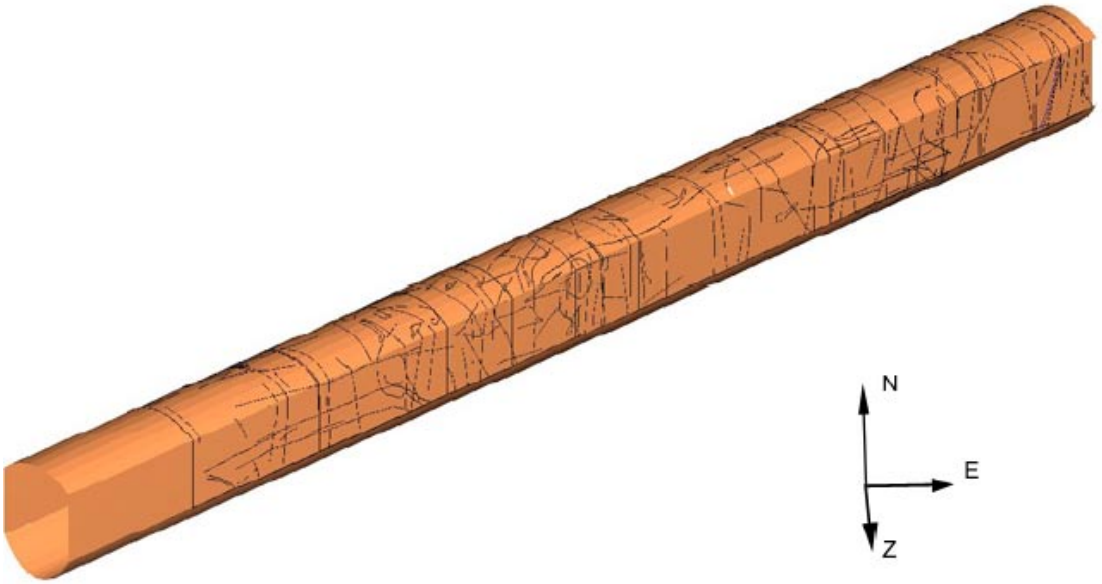


***Figure 2-1.*** *3D-visualisation of fractures in the TASQ tunnel. The first 10 m are not mapped.*

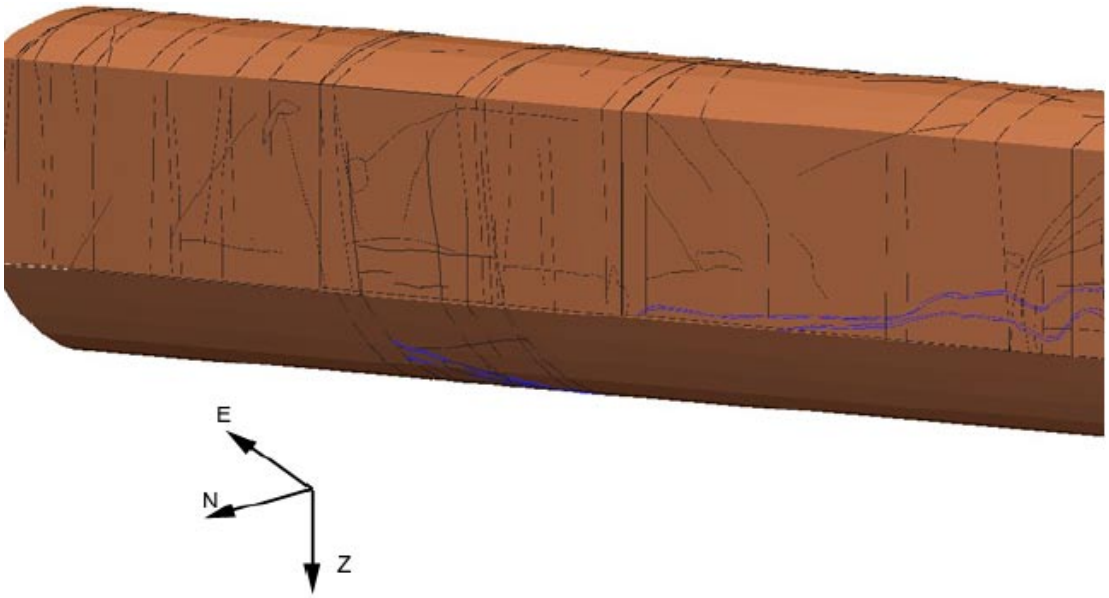


***Figure 2-2.*** *3D-visualisation of the fractures in the TASQ target area for the pillar. The blue undulation lines indicates the shear zone.*

As can be seen in Figure 2-3 the shear zone is divided into two main branches at the target zone for the experiment. The south branch is cutting through the upper part of the pillar volume. A projection of the shear-zone and fractures in the vicinity of the pillar volume 0.5 m below the tunnel floor is presented in Figure 2-4.

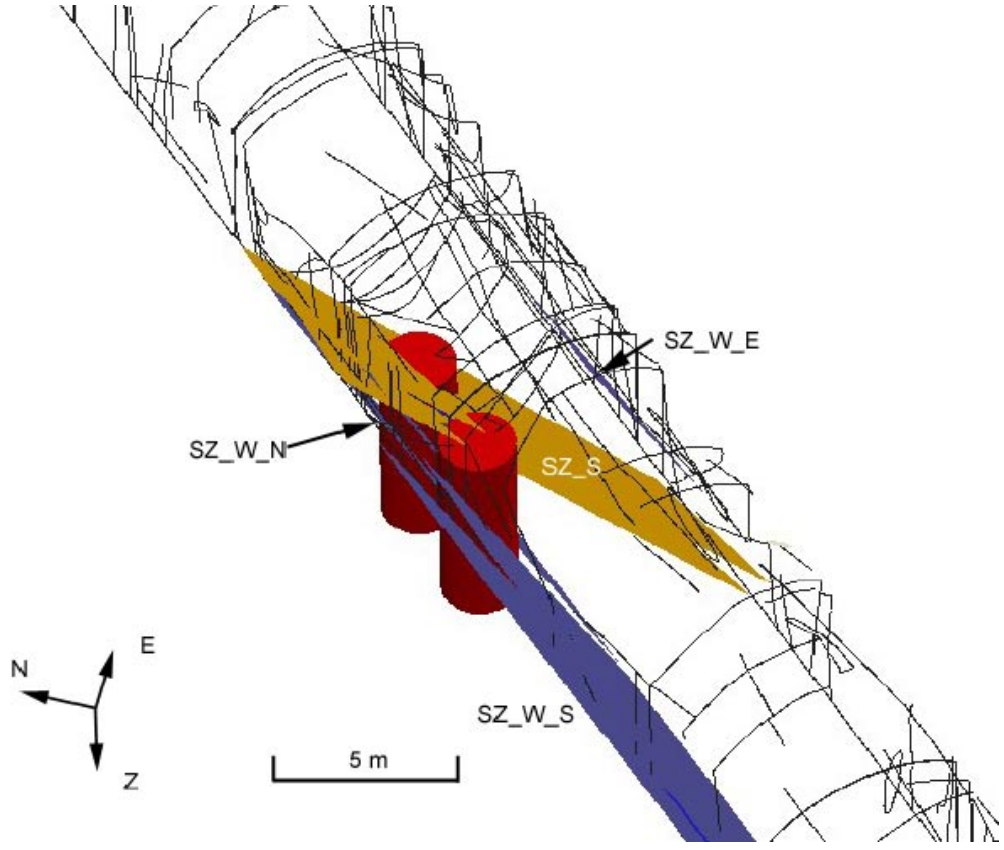


***Figure 2-3.*** *Visualisation of the two main branches of the shear zone in the target volume. The yellow south branch cuts through the upper part of the pillar volume. The red cylinders represents the location of the two large holes planned.*

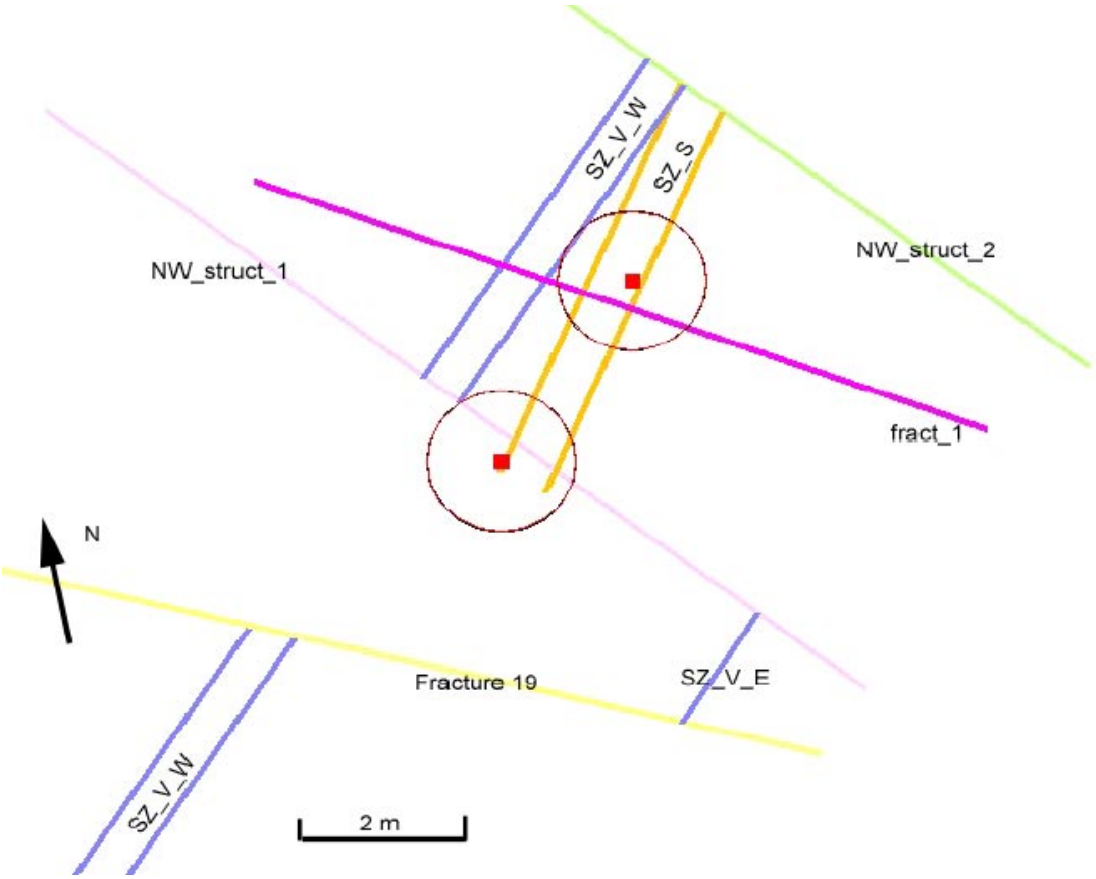


***Figure 2-4.*** *Horizontal projection of the discontinuities at 0.5 m below the tunnel floor.*

There was one major concern that was thoroughly discussed before the target volume was chosen according to Figure 2-3 and Figure 2-4. The strength of the sheared brittle ductile oxidized rock is lower than for the diorite. Especially the contacts with the ordinary diorite are weak due to mylonitization. When the upper part of the pillar is subjected to high stresses it was discussed if slipping along the contacts that would re-distribute the stresses. This could result in too low induced stresses in the hole wall to induce spalling. It was also discussed if the weak rock in the shear zone could start to yield. The associated deformations could then re-distribute the stresses endangering the possibility to initiate spalling. The final assessment of the situation was however that the properties of the shear-zone would not endanger the outcome of the experiment. The initial target area was then finally chosen for the pillar.

A number of rock mechanical parameters were derived during the characterization process that was used as input data for the numerical models. A summary of the parameters are listed in Table 2-1 and Table 2-2.

**Table 2-1. Mechanical and thermal properties of intact Äspö diorite used in the numerical models in the APSE project.**

| Parameter | Mean value | Unit | Standard variation |
|---|---|---|---|
| Uniaxial compressive strength, low | 130 | MPa | |
| Uniaxial compressive strength, high | 210 | MPa | |
| Young's modulus, intact rock | 76 | GPa | 6.5 GPa |
| Young's modulus, rock mass | 55 | GPa | |
| Poisson's ratio, intact rock | 0.25 | – | |
| Poisson's ratio, rock mass | 0.26 | – | |
| Friction angle, intact rock | 49 | Degrees | |
| Friction angle, rock mass | 41 | Degrees | |
| Cohesion, intact rock | 31 | MPa | |
| Cohesion, rock mass | 16.4 | MPa | |
| Tensile strength | 14.3 | MPa | |
| Thermal conductivity | 2.60 | W/m, K | |
| Volume heat capacity | 2.10 | $MJ/m^3$, K | |
| Linear expansion | 7.0E–06 | l/K | |
| Density | 2.731 | $g/cm^3$ | |
| Initial temperature of the rock mass | 15 | °C | |
| Crack initiation stress | 121 | MPa | |
| Crack damage stress | 204 | MPa | |

**Table 2-2. Mean values of mechanical fracture properties used in the fracture models.**

| Parameter | Mean value | Unit | Standard variation |
|---|---|---|---|
| Mode I toughness, KIC | 3.8 | $MPa/m^{1/2}$ | 0.1 $MPa/m^{1/2}$ |
| Mode II toughness, KIIC | 4.4 to 13.5 | $MPa/m^{1/2}$ | |
| Initial normal fracture stiffness, KNI | 175 | GPa/m | 68 |
| Normal fracture stiffness, KNH | 26,976 | GPa/m | 22,757 |
| Shear stiffness | 15.7 / 35.5 | GPa/m | |
| Residual angle | 31 / 30 | Degrees | |

The in-situ stress tensor in the experiment volume is a boundary condition for the experiment and hence important for the success of the experiment, as described in the section about the experiment design in Section 3 in this report. A compilation of available rock stress measurements in the vicinity of the experiment volume was used for the early scooping calculations of the experiment. The stress data was later refined using results from convergence measurements made during the excavation of the tunnel. The stress field used for the final modelling is presented in Table 2-3. The interpretation of the convergence measurements were though refined during the final modelling phase and the stress tensor was slightly changed. The resulting stress tensor is given in Table 2-4.

**Table 2-3. Stress tensor used for the numerical modelling using a Young's modulus of 55 GPa.**

| | Magnitude (MPa) | Trend/Plunge (degrees) |
|---|---|---|
| Sigma 1 | 27 | 310/07 |
| Sigma 2 | 15 | 090/83 |
| Sigma 3 | 10 | 208/00 |

**Table 2-4. Final stress field derived for the experiment volume by back-calculation of the convergence measurements using a Young's modulus of 55 GPa. The final results were not completed in time to be used for the final numerical modelling.**

| | Magnitude (MPa) | Trend/Plunge (degrees) |
|---|---|---|
| Sigma 1 | 30 | 310/00 |
| Sigma 2 | 15 | 090/90 |
| Sigma 3 | 10 | 208/00 |

If scooping calculations are made with 3D models using the two slightly different stress tensors listed in Table 2-3 and Table 2-4 the difference is small. It was therefore decided not to re-run the models using the final stress tensor derived from the back analyze.

# 3 Design of experiment

The experiment was designed in several different steps as listed below. In summary the rock strength and the in-situ stress field was assessed and this data was used to determine how much the in-situ stress should be increased without reaching critical stress limits that could initiate brittle failure. The stress increase was achieved using the geometry of the tunnel, the hole spacing and elevated temperature. It could then be assessed how much heating that was necessary to initiate the spalling process and the heaters were designed accordingly.

- Study of rock mechanics data.
- Calculations of suitable geometries to increase the stress in the experiment volume.
- Choice of pillar width (spacing between the deposition holes).
- Design of the heating system.
- Choice of experiment location at the Äspö HRL.

Results from rock mechanics testing of cores from the Äspö HRL were studied. The uni- and tri-axial testing indicated that the crack initiation strength of an intact unconfined piece of rock is approximately 121 MPa. At this stress level the rock enters the transitional zone and the micro fracturing rate accelerates. It was decided that the geometry of the experiment volume should be designed so that the first metre of the hole walls of the large holes should be stressed to at least 121 MPa after excavation. The stress increase by the thermal expansion should then force the rock to spall.

Calculations was performed to design a suitable shape of the experiment drift. Since the large holes should be placed in the centre of the tunnel an arched tunnel floor geometry was chosen. An evenly distribution of stress in the tunnel floor is now achieved.

When choosing the pillar width there are three important variables to bear in mind; stress, scale and natural fractures. The closer the boreholes are located together the higher the stress concentration becomes. It is though not suitable to have a discrete fracture passing through the pillar since it probably would give undesirable effect on the outcome of the experiment. The relative size of discontinuities in the pillar compared to the pillar width is therefore of importance.

As abovementioned the crack initiation stress is assessed to 121 MPa and the objective with the design was to reach this stress level at 1 m below the tunnel floor after the excavation of the holes. To ensure spalling to take place it was assessed that the stress in the hole wall should be at least 150 MPa. The extra 30 MPa is added by thermal expansion of the rock due to the heating with electrical heaters placed outside the pillar volume. Scooping calculations were performed to determine the needed heater effect and the most suitable placement and number of electrical heaters to be used.

The scooping calculations for the geometry design used a conservative 25 MPa magnitude for the major principal stress. Since the geometry of the experiment concentrates the in situ stress about six times at the hole walls, small changes in the stress tensor gives quite large changes on the stress at the hole walls. To ensure that the in situ stress should be at least 25 MPa the experiment had to be located at the 450 m level at the Äspö HRL.

## 3.1 Choice of geometry

The numerical tools used for the calculations of the geometry were the boundary element code Examine3D and the finite element code Phase2 by Rocscience Inc. /Andersson, 2003/. The input data used for the scooping calculations is somewhat different compared to what is presented in the geology section herein since no site specific data was available at that time. Instead conservative values on the stress tensor and rock properties were chosen. The scooping calculations therefore in principle give a worst case scenario. Two different geometries of the experiment were modelled simultaneously. The first model was a straightforward geometry with two holes close to each other. The second model included slots cut in each of the two hole walls opposite the pillar. The thought with the slot was to concentrate in situ stresses from a larger area and hence further increase the stresses in the pillar walls. The two models are presented in Figure 3-1.

To get an even distribution of the stresses in the pillar volume the tunnel floor was arched with the radius 2.5 m. The height of the tunnel was set to 7.5 m to get the stresses in the floor high enough. Figure 3-2 presents the stress distribution in a vertical plane for the 7.5 m high tunnel with and without the arched floor. The effect is obvious.

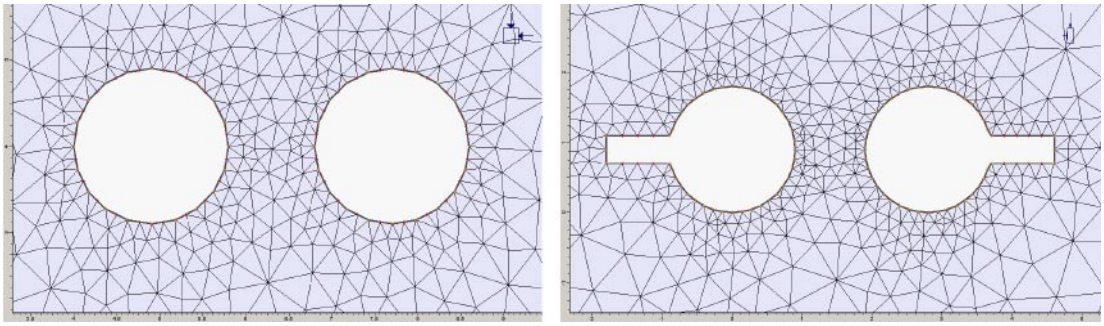

***Figure 3-1.*** *The two different models used in the scooping calculations, one with and one without slots. The slots in the model are 0.9 m deep.*

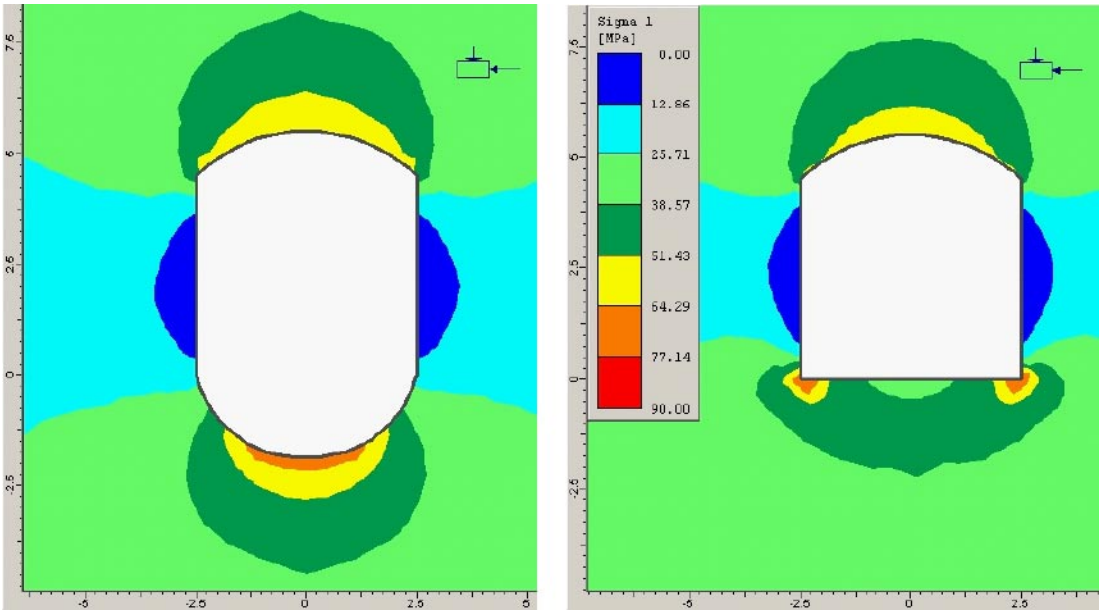


***Figure 3-2.*** *Stress distribution around a tunnel section with and without an arched floor. The arch nicely concentrates the stresses in the centre of the tunnel floor giving an even stress distribution throughout the section.*

## 3.2 Choice of pillar width

The pillar width was determined by a balancing the obtained stress increase, the risk for a natural fracture to cut through the entire pillar and the scale. With scale means that if the pillar width is chosen too narrow its response will be sensitive to small discontinuities. A narrow pillar will be more stressed, but on the other hand, sensitive to the small scale geology in it. A wide pillar will be less stressed but will react more like a rock mass. The risk for a natural fracture cutting through a wide pillar is of course also smaller for a wide pillar. The cumulative part of a total number of 1,727 fractures mapped at the Äspö HRL is plotted against their trace length in Figure 3-3. As can be seen there 65% of the fractures have a trace length of 1 m or less and the slope of the curve is almost linear. The fracture intensity for fractures with trace lengths longer than 1 m is rapidly decreasing.

The width of the pillar was chosen to 1 m since it was assessed that the sensitivity to discontinuities with a size up to 30 cm is rather low and the chance for a random fracture to cut through the entire pillar is about 35%.

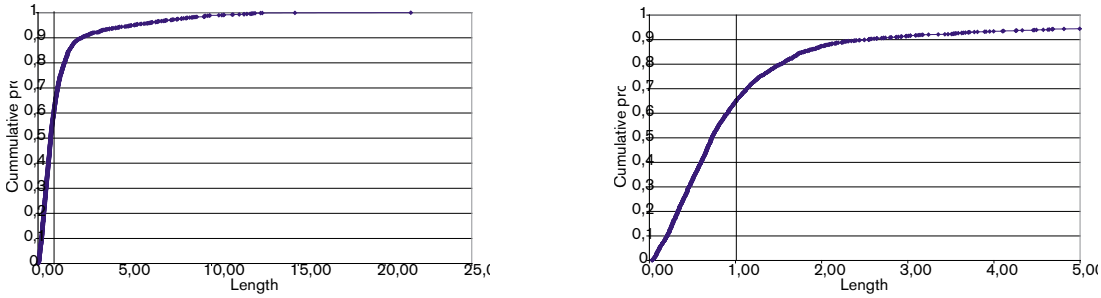


***Figure 3-3.*** *Plots of cumulative part of fractures versus trace length. The only difference between the two plots is the scale on the X-axis. The vertical line indicates a trace length of 1 m.*

## 3.3 Heating system

As stated in the section about the scooping calculations it is assumed that the thermal induced stress in the pillar should be at least 30 MPa to make sure that spalling is initiated. Other pre-requisites for the heating system is that the heaters shall make an as small impact on the acoustic emission monitoring as possible and that the temperatures in the rock at the sensor locations have to be lower than what is specified for the electronics. In Figure 3-4 the chosen geometry is stated and in /Staub et al. 2003/ the modelling made to reach this decision is presented.

The chosen geometry is favoured by the facts that the heaters are located outside the acoustic emission monitoring downhole equipment and that four heaters gives a more evenly distributed heat front through the pillar than for example what one heater on each side would do. The effect of 200 W/m will give temperatures below the critical limit for the electronic equipment.

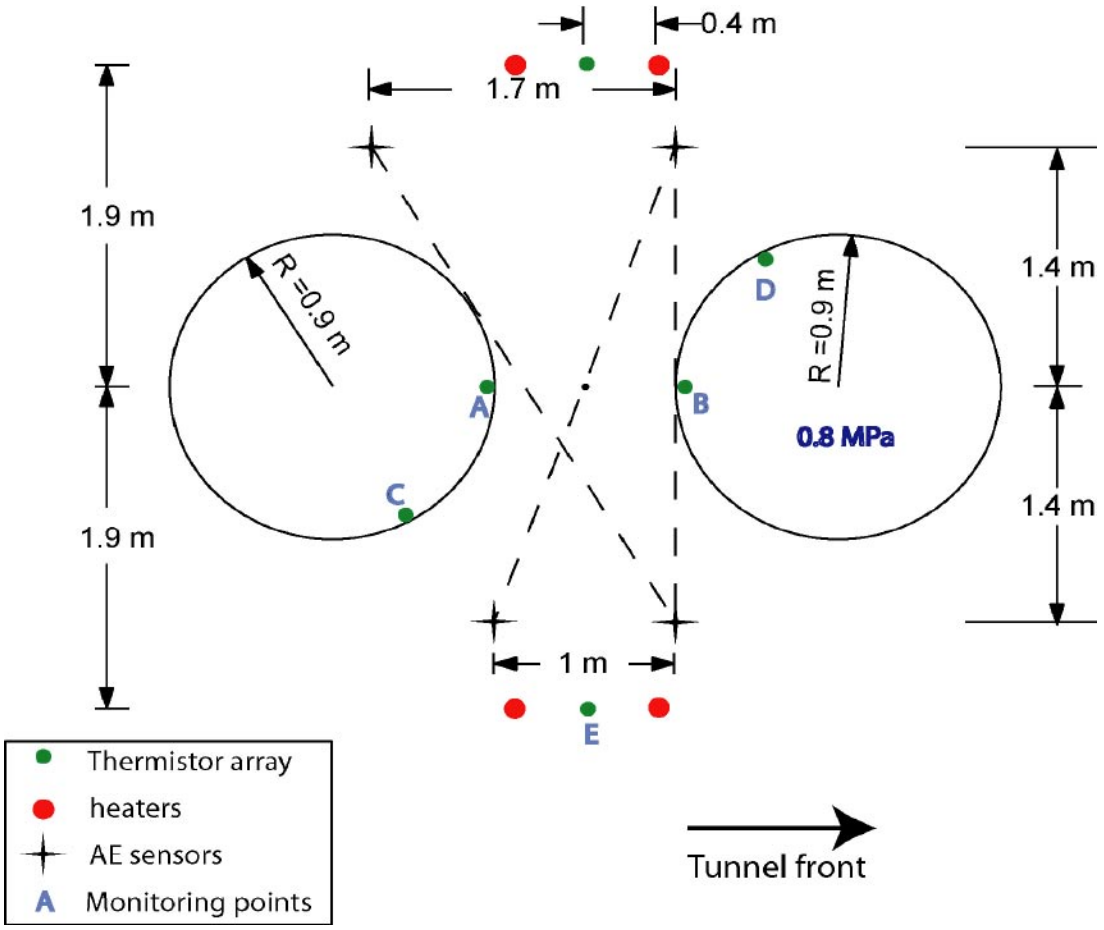


***Figure 3-4.*** *Layout of the heaters and the acoustic emission system. The effect of the heaters is 200 W/m and the heaters should be at least as long as the large holes are deep so that the entire pillar wall is heated.*

### 3.3.1 Equipment and installation

The electrical heaters purchased for the experiment can give an effect of 460 W/m over a 6.5 m length which gives a redundancy of more than 100% regarding the possibility to heat the rock to the right temperature. If necessary, each of the four heaters can be coupled to its own thyristor and hence individually controlled. Thereby it will be possible to compensate for different conditions in the holes i.e. different water flows. The power output from each thyristor is monitored by the data acquisition system set up for the experiment presented in Section 4.

To protect the heaters from the extreme corrosive environment the hot salty water creates each heater will be placed inside a cupper tube. The tube will only have an opening at the top and the heater element will therefore only come in contact with air. The slot between the cupper tube and the borehole wall will be filled with fine grained sand that will be saturated. The diameter of the bore hole is 76 mm and the diameter of the cupper tube is 25 mm. In Figure 3-5 a heater placed next to the protective cupper tube and installed heaters are presented. To give good heat transportation abilities between the heaters and the rock the borehole with the heaters is filled with fine-grained sand.

***Figure 3-5.*** *Left: photograph of heater element placed next to the protective cupper tube. Right: heaters inside cupper tubes installed in borehole which later was filled with sand.*

## 3.4 Confinement

An important part of the experiment is the study how confinement pressure effects the strength of the rock mass. Water was chosen to apply the confinement pressure in one of the holes. Since the pressure in the confinement equipment shall be 0.8 MPa it is necessary to have a membrane between the water and the rock wall to prevent water from leaking through fractures. The membrane needs to be rather flexible to avoid point loads on the hole wall and thus give an even pressure. It is also necessary to make a construction that keeps the pressurized water in the hole. The construction is not trivial since the area of the hole is approximately 2.5 $m^2$, a 0.8 MPa pressure working on that area gives a force of 2,000 kN. Two different types of constructions were discussed for this task. The first was a steel lid anchored with steel cables grouted into boreholes in the floor of the tunnel. The idea was discarded since a force that could be difficult to define would be applied to the rock volume close to the pillar. This could possibly make the numerical modelling results more difficult to evaluate. The holes that would be needed for the wires could also effect the acoustic emission system and be in the way for other instrumentation. It is not possible to take the reaction force in the tunnel roof since the drilling machine will stand over the pressurized hole when drilling the second pillar hole. The second construction, which was chosen, was self bearing and would hence not need to be fastened to the rock. The general idea with the construction is to use a rubber bladder as a membrane. The bladder is confined by steel lids in the top and bottom connected with load bearing textile straps. The construction is visualised in Figure 3-6 to Figure 3-9. The length of the total package is approximately 6 m. It is very important that the rubber bladder is totally confined by the steel and textiles. If there is a tiny opening somewhere in the construction the rubber will expand through it and burst due to the high pressure.

A pressure vessel filled with water connected to a Nitrogen gas tube via a pressure reducing valve is connected to the steel lid and the rubber bladder by a flexible hose. The pressure reducing valve is set to the appropriate pressure, 0.8 MPa in this case, and the same pressure will be transferred to the bladder. During the heating of the pillar the water will expand, to maintain the pressure in the bladder water has to be released from it to protect the integrity of the construction. This will mainly be done by hand but a safety valve is put on the lid just in case. A pressure transducer will be placed on top of the steel lid. The transducer will be connected to the data acquisition system enabling a constant monitoring of the pressure in the hole.

***Figure 3-6.*** *Left figure: the confinement equipment that will host the rubber bladder membrane, right: Microstation drawing of the equipment. The load bearing textile straps are orange/red in the construction and yellow in the drawing.*

***Figure 3-7.*** *Photograph of the steel lids.*

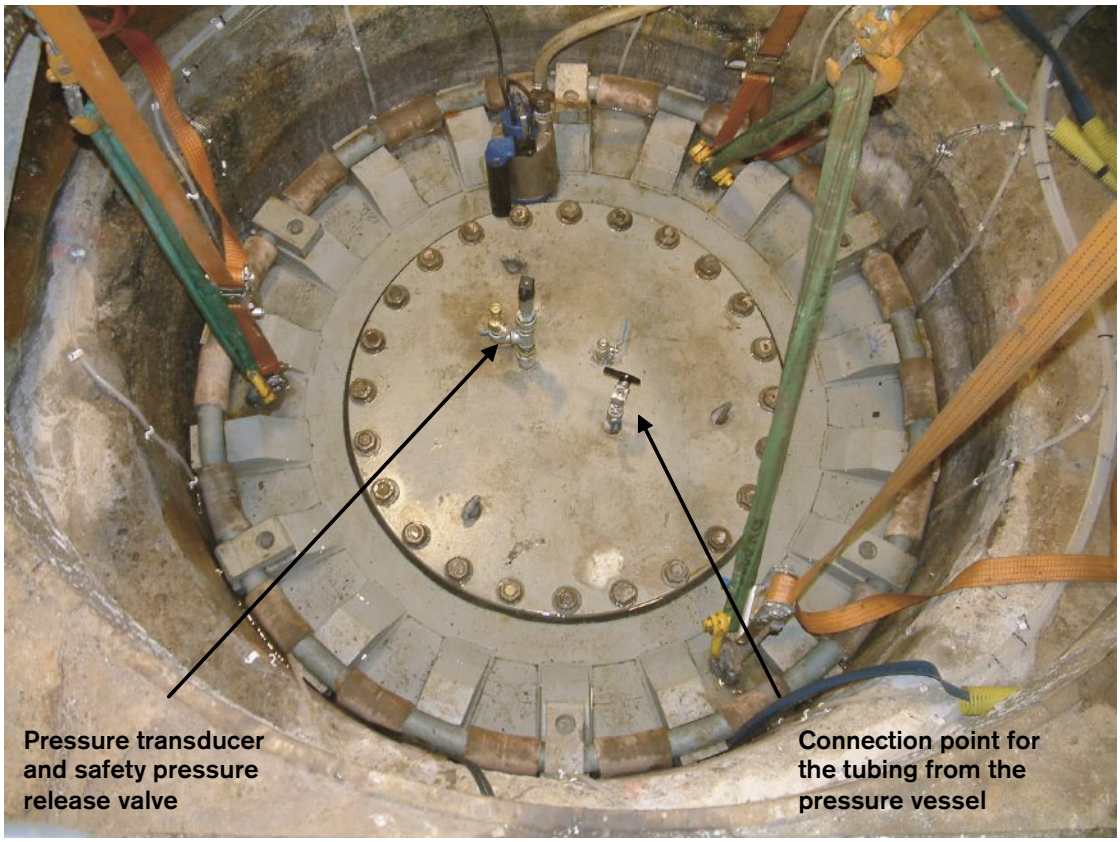


***Figure 3-8.*** *Photograph of the top steel lid with man-hatch after installation. Note the placement of the pressure transducer, the safety valve and connection point for the tubing from the pressure vessel.*

***Figure 3-9.*** *Photograph of the pressure vessel and the accompanying gas tube. The flexible Tecalan tube in the photograph is connected to the bladder via the top steel lid and ensures the pressure in the bladder even if there is a small water leakage through the sealing around the man-hatch in the lid.*

# 4 Monitoring

One of the objectives with the experiment is that "our current capability to predict spalling in a fractured rock mass" is to be demonstrated. To be able to validate the numerical models with the actual behaviour of the rock mass it is of course necessary that the models deliver predictions that can be measured in the field. It was therefore specified that all predictions should contain displacements and temperatures over time.

The measuring of temperature is a quite simple task since the thermo-couples easily can be mounted in core boreholes or any other borehole down to a diameter of 5 mm. The measuring of the displacements on the rock surface of the open hole is though a more challenging task since:

- The increasing temperature effect the gauges and they need to be calibrated for the entire temperature span.
- The environment is extremely hostile to electronic equipment with temperatures up to 70 degrees C, a RH of about 100% and possibly dripping of saline water.
- The elastic displacements will be in the range of 1 mm. The small displacements and the environment demands both very accurate and robust sensors. The small displacements also make strict requirements on how the instruments are mounted and on what. The rock surface in the entire hole will move both horizontally and vertically which makes it difficult to maintain a true "zero point" for the transducers.
- The spalling will probably make smaller slabs of rock to fall down from the hole walls. The instruments need to be protected from those kinds of incidents.

The thermal and displacement monitoring is detailed described in /Andersson and Eng, 2005/.

## 4.1 Strategy

The strategy with the monitoring is that the rock's response to the loading should be followed both inside the pillar volume itself and on the rock surface of the open hole. To get a measure of the thermal loading thermocouples are an important part of the instrumentation.

An important system is the monitoring inside the rock volume. An acoustic emission (AE) system has been chosen for this task. The AE system can locate within centimetres where inside the rock volume fractures are induced and follow the propagation of these fractures or propagation of existing fractures that starts to slip. The system is also used for ultrasonic surveys which gives a relative measure of the density of the micro fracturing and how it changes close to the hole walls when the stresses are increased by the applied thermal load.

The displacements on the rock surface of the open hole will give a good insight in how well the numerical models can predict small displacements. The monitoring will also give a good insight in the volumetric change of the rock when the spalling starts to slab parts of the pillar wall. It is probably unique for this project that the displacements are measured through the elastic phase and during the initiation, and propagation of the spalling process.

The temperature measurements are a quite straight forward task. Gauges are placed so that the temperature can be monitored symmetrically around the pillar. The results from the measurements will during the experiment's heating phase be used to control that the heat front is symmetrical, if not: the effect on one or several of the heaters can be adjusted individually.

It was decided to perform the modelling of the experiment in two different levels located 0.5 m and 1.5 m below the tunnel floor. The reason was that it is very likely that relative extensive spalling will be initiated at the 0.5 m level. At the 1.5 m level it is anticipated that more moderate spalling will occur. To place the instruments at these two levels it is assessed that a good cover of the spalling process is achieved. The choice of two instrumented levels makes it necessary to conduct numerical modelling of the two levels.

To make a thorough evaluation of the experiment possible the readings from all the instruments needs to be properly handled. All transducers are connected to a data scan system that logs the measured values with a suitable scan rate. Depending on the phase the experiment is in the scan rate is easily changed. The pressure in the confining equipment as well as the effect of each heater is also stored in the system which is connected to the SKB LAN. The experiment can in detail be followed from surface at Äspö HRL or anywhere else an internet access point is found. The acoustic system works on a separate system outside the SKB LAN, though accessible by a modem connection, data from that system containing i.e. the number of events and their co-ordinates will be downloaded every day to the SKB system.

## 4.2 Transducors for displacement monitoring

In /Andersson and Eng, 2005/, the process for choosing the instrument types and their mounting system for the displacement measurements is described in further detail.

The transducers chosen for the displacement monitoring are of LVDT (Linear Variable Differental Transformer) type. The sensor type is accurate and robust to withstand the harsh climate in the deposition hole. Two types of LVDTs will be used in the experiment. This is necessary since it is of interest to measure the elastic as well as brittle deformations at the hole wall. The elastic deformations are very small, in the magnitude of 1 mm. To get good readings the instrument used needs to be very sensitive for small movements; the fine resolution though gives a small measuring range for the instrument. Half of the LVDTs will therefore be of this type with a measuring range of approximately 12 mm. To measure the larger displacements that will take place during the spalling of the hole wall another, a bit less accurate type will be used but the measuring range will be 40 mm. At each of the two levels that will be monitored there will be 6 LVDTs of the respective type making up totally 24 LVDTs in the open deposition hole. It is assessed that these two types of instruments will complement each other well and give good measuring series. All LVDTs that are used have been checked and calibrated for the temperature increase they will be subjected to.

The short range high resolution LVDTs are made by Schaevitz. Their resolution is 0.001 mm with the used configuration. The long range LVDTs are made by Geometric and their resolution is 0.003 mm. A photograph of the two types is presented in Figure 4-1.

The preliminary geometrical placement of the LVDTs along the hole wall is illustrated in Figure 4-2. The transducers at each level will cover a sector of 60 degrees, 30 degrees on each side of the pillar centre. The measuring will be done at 6 discrete points evenly

distributed along the sector. The vertical spacing between the long and short range transducers will be approximately 10 cm. The spacing is necessary since the electronics in the two types of instruments might interfere with each other resulting in disturbed and fluctuating readings.

Since the displacement of the hole wall is to be measured the LVDTs have to be mounted so that their fastenings are independent of these movements. The supporting construction is not trivial because of the increasing temperature in the hole. The chosen construction in presented in the following section.

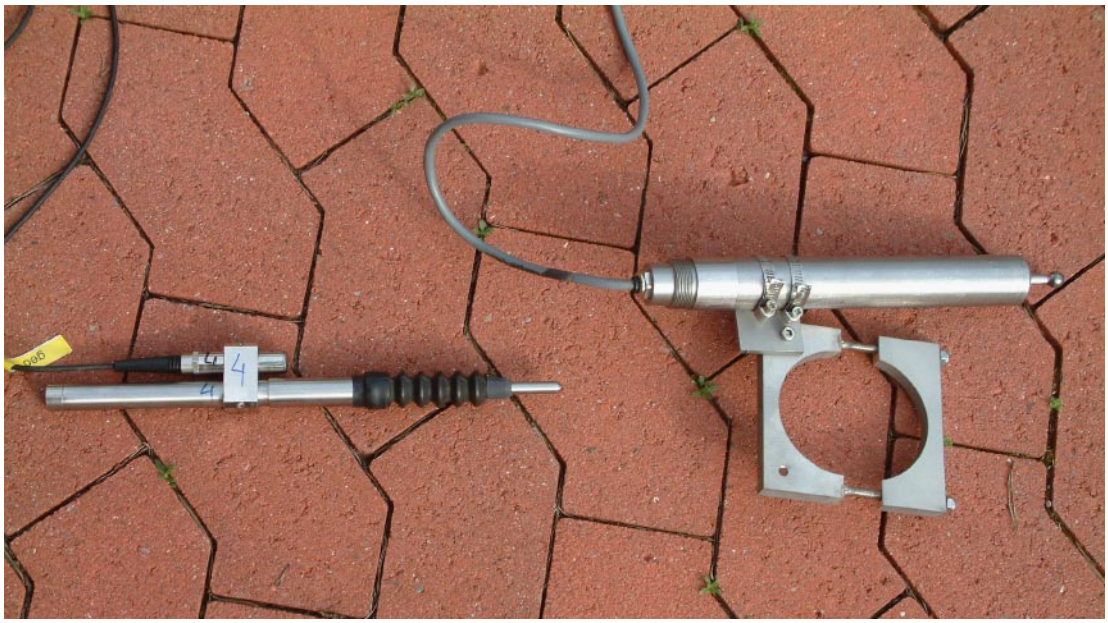

***Figure 4-1.*** *Photograph of the two LVDT types. Left the long range model and right the short range model. The short range model is attached to the equipment that will be mounted on the supporting construction consisting of vertical steel pipes along the pillar wall.*

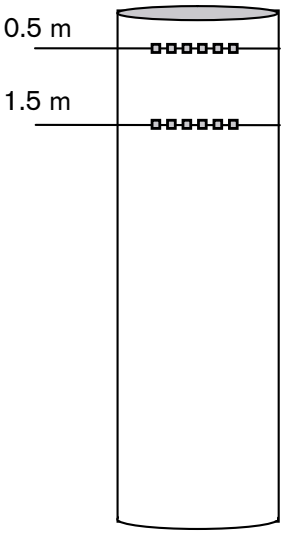


***Figure 4-2.*** *Illustration of geometrical placement of the LVDT transducers along the deposition hole wall. The actual depth placement of the sensors might change when the actual geology of the hole is mapped. Each square represents one long range and one short range LVDT making up totally 24 LVDTs.*

### 4.2.1 Supporting construction for the LVDTs

It is not practical to make a supporting device for the LVDTs that is not effected by the temperature increase in the deposition hole. The strategy chosen therefore is to make a device whose behaviour can be kept under reasonable control. The major part of the construction will therefore consist of three vertical 6 m long steel pipes. The pipes will be fastened in the bottom of the hole where the rock movements are assessed to be insignificant. At the top of the hole a steel beam is bolted to the rock in which the steel pipes are supported. The upper support is constructed so that the pipes are free to move vertically but not horizontally. The thermal expansion of the pipes will therefore not induce stresses into the pipe. Photographs of the support are presented in Figure 4-3.

One could argue that the beam used for the upper support will expand during the heating and slightly move the pipes. To handle this, the beam and its bolting to the rock have been designed to withstand the deformation due to thermal expansion. The beam will stay in a fixed position and the temperature will only increase the stress inside the beam and not displace it.

It is not sufficient to only support the 6 m long pipes at the top and bottom. The pipes will be deflected by the springs in the LVDTs when they are mounted. Additional support is therefore added close to the measuring levels. This support will stabilize he pipes horizontally but will allow vertical displacement due to the thermal expansion. The support construction is illustrated in Figure 4-4.

The beams for the construction in Figure 4-4 are placed perpendicular to the tunnel axis in the centre of the deposition holes. This placement has been chosen since the displacement of the hole wall will be parallel to the beam and not displace it along the tunnel axis. The support for these two beams will be constructed so that the small displacement of the rock wall or the thermal expansion not will displace the beam. The thermal expansion of the steel plates that are fastened in the beam and support the pipes will though move the pipes slightly. To compensate this, the temperature monitoring will be used to calculate the expansion of the plates and the LVDT readings will be compensated with these numbers. This method is assessed to be more precise than using strain gauges or LVDTs mounted on the steel plates.

***Figure 4-3.*** *Lower (left) and upper (right) support for the vertical steel pipes. The pipes can be individually adjusted in height by using the nut the pipe is resting on at the lower support. Vertical movement due to thermal expansion is allowed through the upper support.*

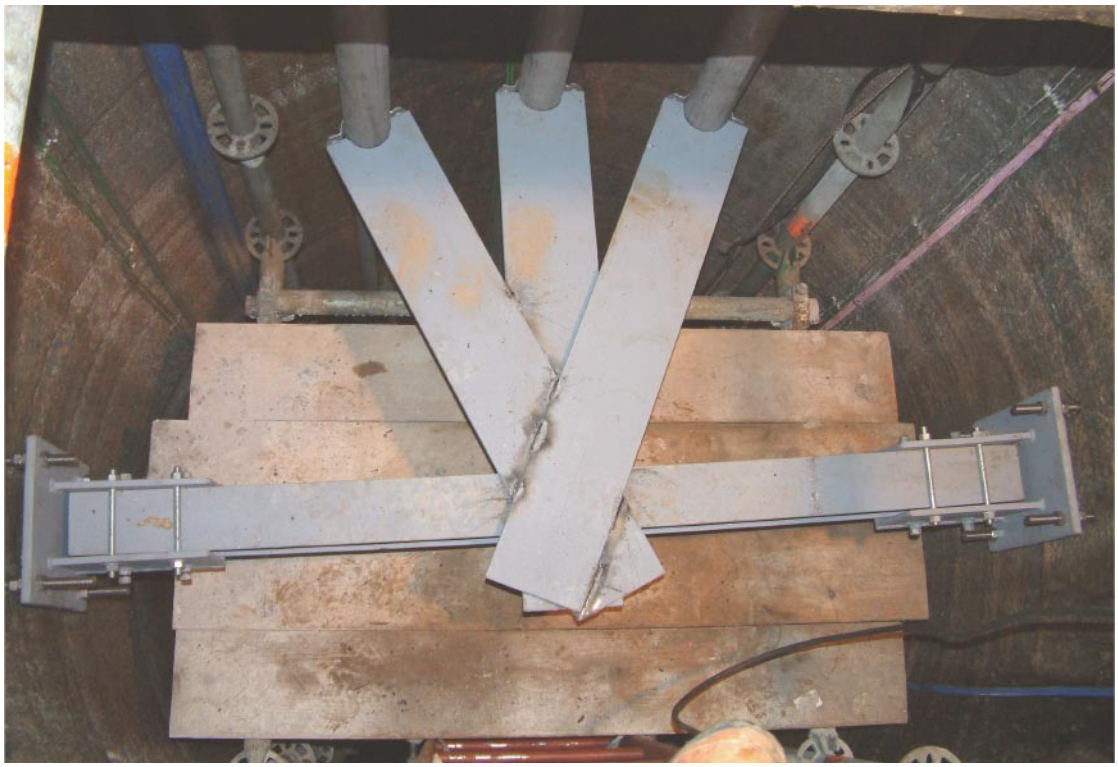

***Figure 4-4.*** *Photograph of the horizontal support of the vertical steel pipes close to the monitoring levels.*

## 4.3 Temperature monitoring

For the temperature monitoring thermocouples are used. The thermocouples are placed both in the pillar walls and in boreholes outside the pillar volume. The thermocouples in the pillar walls are inserted in approximately 30 mm ∅5 mm deep boreholes into the wall to ensure that the actual rock temperature is measured, Figure 4-5.

The transducers are geometrically placed so that it is possible to follow the heat front around the pillar. If it turns out that the temperature field is asymmetrical the heaters can be adjusted individually to compensate for this. The stress increase in the pillar will then be close to what has been modelled and the comparison between the modelled and the actual results will be easier. The placement of the thermocouples in the experiment volume is illustrated in Figure 4-6. The main sensor levels are 1.5, 3.5 and 5.5 m below the centre part of the tunnel floor. A hole inclined 60 degrees from horizontal is also instrumented for evaluation of the thermal predicting capabilities at a slightly longer range.

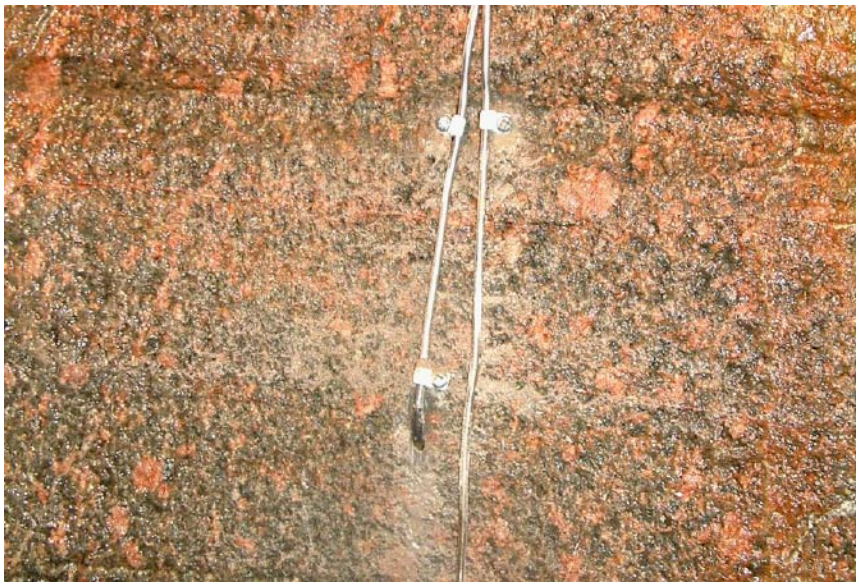

***Figure 4-5.*** *Placement of thermocouple in a small borehole drilled into the pillar wall.*

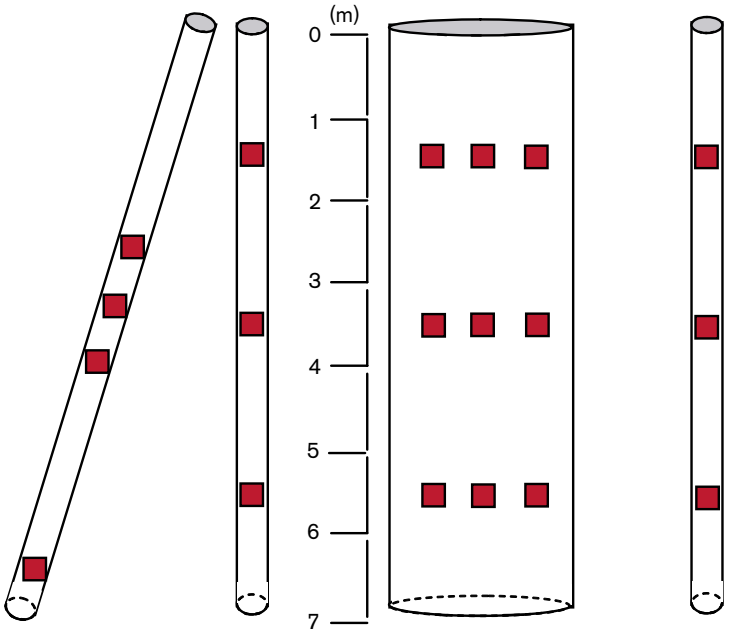


***Figure 4-6.*** *Illustration of the geometrical placement of the thermocouples around the experiment volume.*

## 4.4 Insulation of experiment volume

The 3D-numerical modelling made with FLAC has used a boundary condition where the rock surfaces are adiabatic, fully insulated. To simulate this in the experiment area the tunnel floor around the deposition holes will be insulated up to the tunnel walls. In addition to this a small hut will be erected over the deposition holes. Its walls and roof will also be fully insulated. The hut is constructed so that the hole will be easily accessible for inspection without cooling down the air in it which would had been the case if only insulated lids where placed on top of the hole, Figure 4-7.

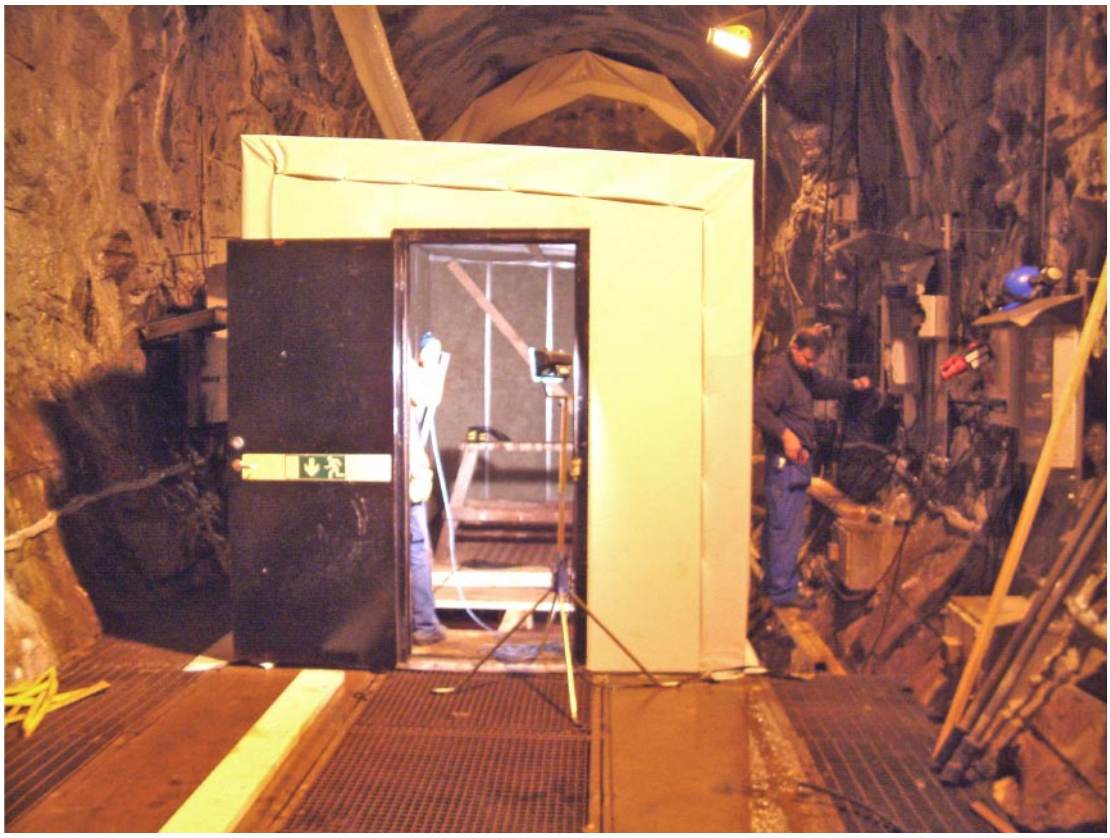

***Figure 4-7.*** *Photograph of the insulating construction on top of the experiment volume.*

# 5 Modelling approach

The numerical modelling for this project has been done in two different phases. The first modelling phase was preformed before the tunnel was excavated. The major objective with this modelling was to confirm that the project could be carried out with a successful outcome. The major concern at this stage was if it was possible to concentrate stresses high enough to induce spalling in the hole walls. At this time no site specific data was available, instead general rock mechanics and stress data from testing made on cores in the vicinity of the experiment volume was used. The uncertainty in the site specific parameter values was handled by including a sensitivity analysis of the most important parameters in the models. In this analysis both extreme values that would give unreasonably low temperature and stresses in the pillar as well as more realistic values where used. The parameters varied were:

- In situ stress, the stress is concentrated about 6 times in the centre of the 0.5 m measuring location.
- Young's modulus, important when the thermal contribution to the stresses is modelled. Has no effect on the elastic modelling of the stresses.
- Thermal conductivity, determines how fast the heating process of the pillar will be.

The sensitivity analysis concluded that even with the lowest case parameters (which are very likely to underestimate the stress in the rock surface of the hole) the induced stresses would be higher than the crack initiation stress. These results encouraged the project and it was given a go ahead. The sensitivity analyses will not be further discussed in this report, details can be found in the preliminary modelling reports by /Fredriksson et al. 2003; Wanne et al. 2003; Rinne et al. 2003/.

As mentioned in the section about the monitoring strategy the instruments will be placed at two levels and hence the predictive modelling has to be made at the same two levels. All predictions are made at 0.5 m and 1.5 m below the tunnel floor.

## 5.1 Numerical tools used for predicitions

For the predictive modelling five different codes where used and are briefly described here. For further information about the codes see the references in Section 6, modelling results.

### 5.1.1 Examine 3D

Examine 3D is a three-dimensional linear elastic boundary element program available from the RocScience Inc (Toronto, Canada).

In the predictive modelling the program was used as a complement to the two-dimensional JobFem code. The geometry of the experiment is too complex to be modelled by a two-dimensional program only. This was solved by using field points in Examine 3D placed in two horizontal planes at 0.5 and 1.5 m below the tunnel floor. The field points where located so that they gave stresses in the nodes of the finite element mesh in JobFem. The stresses in the field points are though given in 3D from Examine3D, they had therefore to be transformed to 2D stresses by a separate algorithm before they where imported to JobFem.

### 5.1.2 JobFem

The numerical code JobFem is based on Finite Element Method. The program has been available for 20 years and used for different applications in the construction sector.

As mentioned above the program used the geometry induced stresses modelled by Examine 3D which were transformed to 2D-stresses which where applied to the nodes in the finite element mesh. The program then calcualtes and applies the thermal stresses to these values resulting in a coupled thermo-mechanical stress field.

The stress derived by the JobFem code is later used in the FRACOD program.

### 5.1.3 FRACOD

FRACOD is a boundary element code for fracture stability analysis in rock material. It has been developed to model fracturing process of the rock material in varying loading conditions. For the APSE project, FRACOD has been updated in many respects including AE simulation. A method to import stresses from other numerical models to FRACOD has also been developed. The method is a reverse stress reconstruction of the nodal stresses in JobFem to boundary stresses in FRACOD.

FRACOD is not used for predictions of the heating phase since it is using its input data from JobFem. But besides deformation predictions the codes major contribution to the project is the analyze of initiation and growth of stress-induced fractures at discrete locations in the pillar

### 5.1.4 FLAC3D

FLAC3D is a finite-difference program which simulates the behaviour of three-dimensional structures built of soil, rock or other materials that undergo plastic flow when their yield limits are reached. The built in programming language FISH was used to enable the analyses that are necessary for this project.

FLAC3D run its complete own model and did not need input from any other numerical code. Besides the predictions specified for the other codes FLAC3D stress results was also coupled to a two dimensional FLAC code. In this process the 3D stress tensor is converted to a 2D tensor. The two dimensional FLAC code is then synchronized to a PFC2D model.

### 5.1.5 PFC2D

The Particle Flow Code models mechanical behaviour by representing a solid as a bonded assembly of circular particles. In order to simulate the APSE with the bonded-particle model, it is necessary to utilize a coupled approach in which an inclusion region comprised of bonded particles is embedded within a continuum grid. The coupling formulation employs the PFC2D and FLAC. The initial stresses and the temperature evolution within the two-dimensional FLAC-PFC2D region are obtained from the elastic thermo-mechanical FLAC3D models with no boreholes and with boreholes and heaters, respectively.

# 6 Modelling results

In this section a summary of the results from the different numerical models are presented in graphs and contour plots. The modellers were also assigned the task to make actual spalling predictions by answering the following four questions:

1. What is the failure criterion, i.e. where does one obtain spalling.
2. What tangential stress is required to initiate spalling.
3. How deep will the spalling propagate.
4. What is the effect of confining stress on 1, 2 and 3 above.

The answers to the questions are summarized here but for a complete description of the different models and their results the interested reader should read the reports used as references in each sub-section.

## 6.1 FRACOD

The FRACOD program is mainly written for modelling of fracture initiation and fracture propagation. For the APSE project the code has been complemented with the possibility to predict the acoustic emission evolution during the fracturing process. In this summary report only the results from the 0.5 m level are presented. The results from the 1.5 m level are similar but of lower magnitudes. All results in this section are from /Rinne et al. 2004/.

FRACOD is at present unable to simulate the effect of thermal loading. Since the problem is thermo-mechanically coupled an alternative approach has been taken. Stresses at certain points in the JobFem-model at different time intervals have been used to reconstruct appropriate boundary stresses. A comparison of the original and the reconstructed stress distributions shows that the difference is very small and does not has to be taken into consideration. This is illustrated in Figure 6-1.

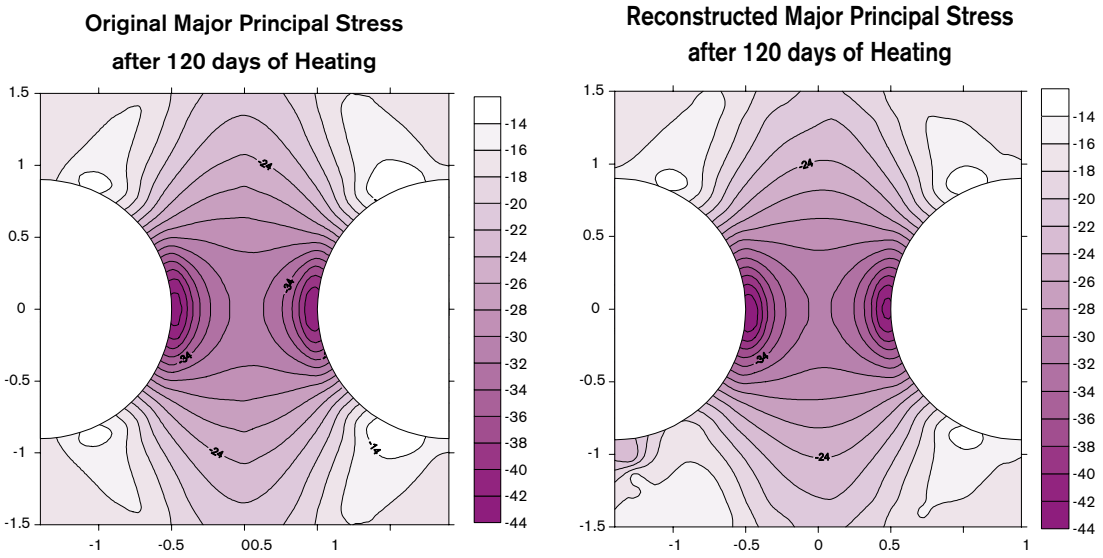


***Figure 6-1.*** *Comparison between the original and reconstructed stress distribution after 120 days of heating. Left: original stress from JobFem, right: reconstructed stress.*

### 6.1.1 Results from intact pillar model at the 0.5 m level

The first fracture propagation model was made under the assumption that the pillar consists of an intact, fracture free rock volume. The results indicate that V-shaped spalled zones can be anticipated to a depth of approximately 10 cm on each side of the pillar. In the open hole the fractured rock will most likely spall off the hole wall. A 80 cm thick core of the pillar will remain intact after the 120 days of heating and the risk for rupturing of the hole pillar is non-existent. The 0.5 m level stress and fracture propagation modelling results are presented in Figure 6-2 and Figure 6-3, in both figures the right hole is confined.

The effect of the 0.8 MPa confining pressure in the right hole in the figures is quite small after 120 days of heating. The effect is more apparent until 60 days of heating. Up to this time the fracture propagation is suppressed by the confinement. When the thermal load if further increased the effect of the confinement is reduced and after 90 days, it is very indistinct.

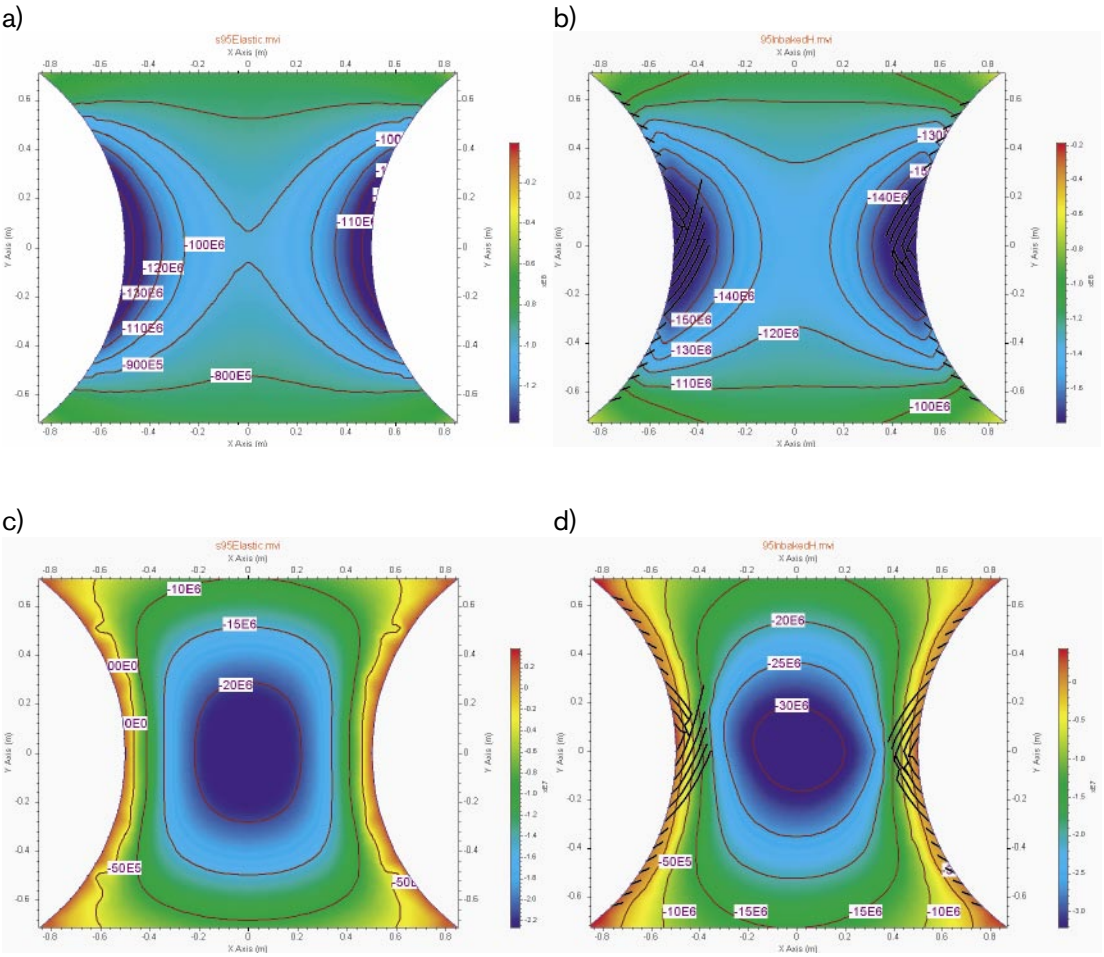


***Figure 6-2.*** *(a) Compressive stress (σ1) distribution caused by excavation before failure. (b) Brittle model after 120 days of heating. (c) Minor stress (σ3) distribution caused by excavation before failure. (d) Brittle model after 120 days of heating.*

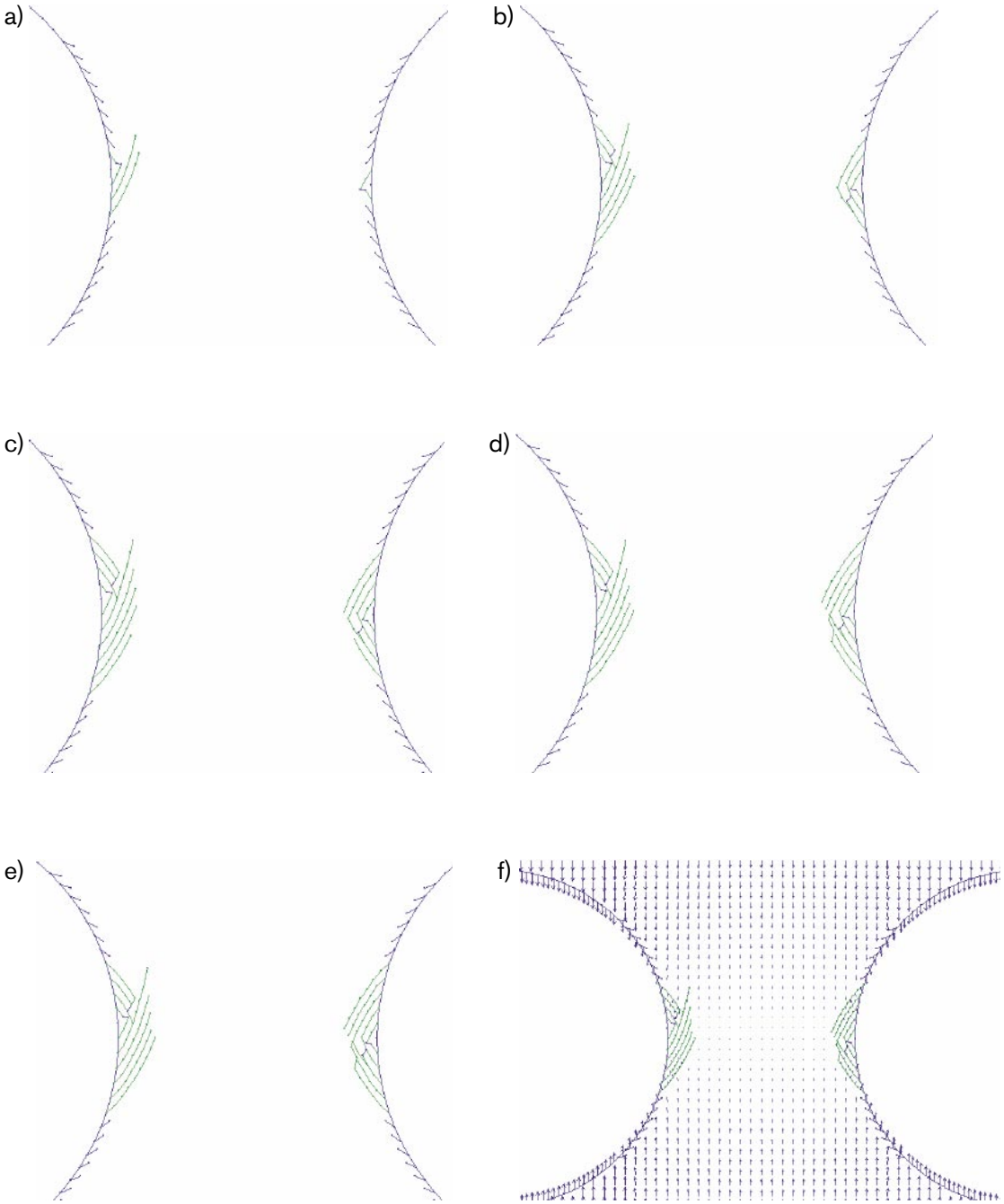


***Figure 6-3.*** *Fracture initiation and propagation at the borehole boundary. Section 0.5 m below the tunnel floor. (a) Fracture pattern after excavation. (b) After 30 days of heating. (c) After 60 days of heating. (d) After 90 days of heating. (e) After 120 days of heating. (f) Displacements after 120 days of heating. See displacements in Table 3-2.*

### 6.1.2 Displacements from intact pillar model at the 0.5 m level

The predicted displacements are rather small. Before the heating has started the largest displacements are predicted to approximately 1.8 mm and after 120 days of heating it have increased with approximately 0.8 mm to 2.6 mm. The deformations along the pillar wall are only a few tenths of millimetres. The difference between the open and the confined hole is so small that it doesn't make any practical difference. The directions of the displacements are defined in Figure 6-4 and the predicted displacements in Figure 6-5.

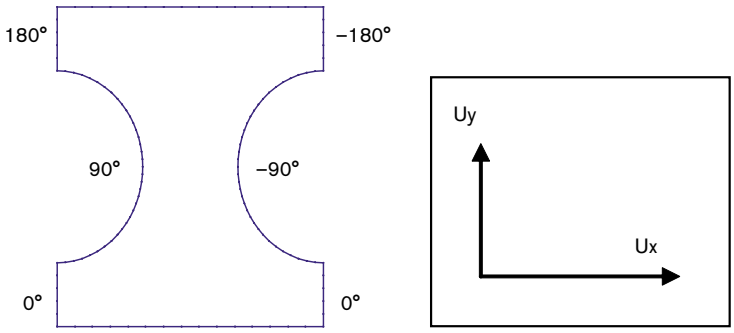


***Figure 6-4.*** *Definition of positive displacement directions of the pillar boundaries.*

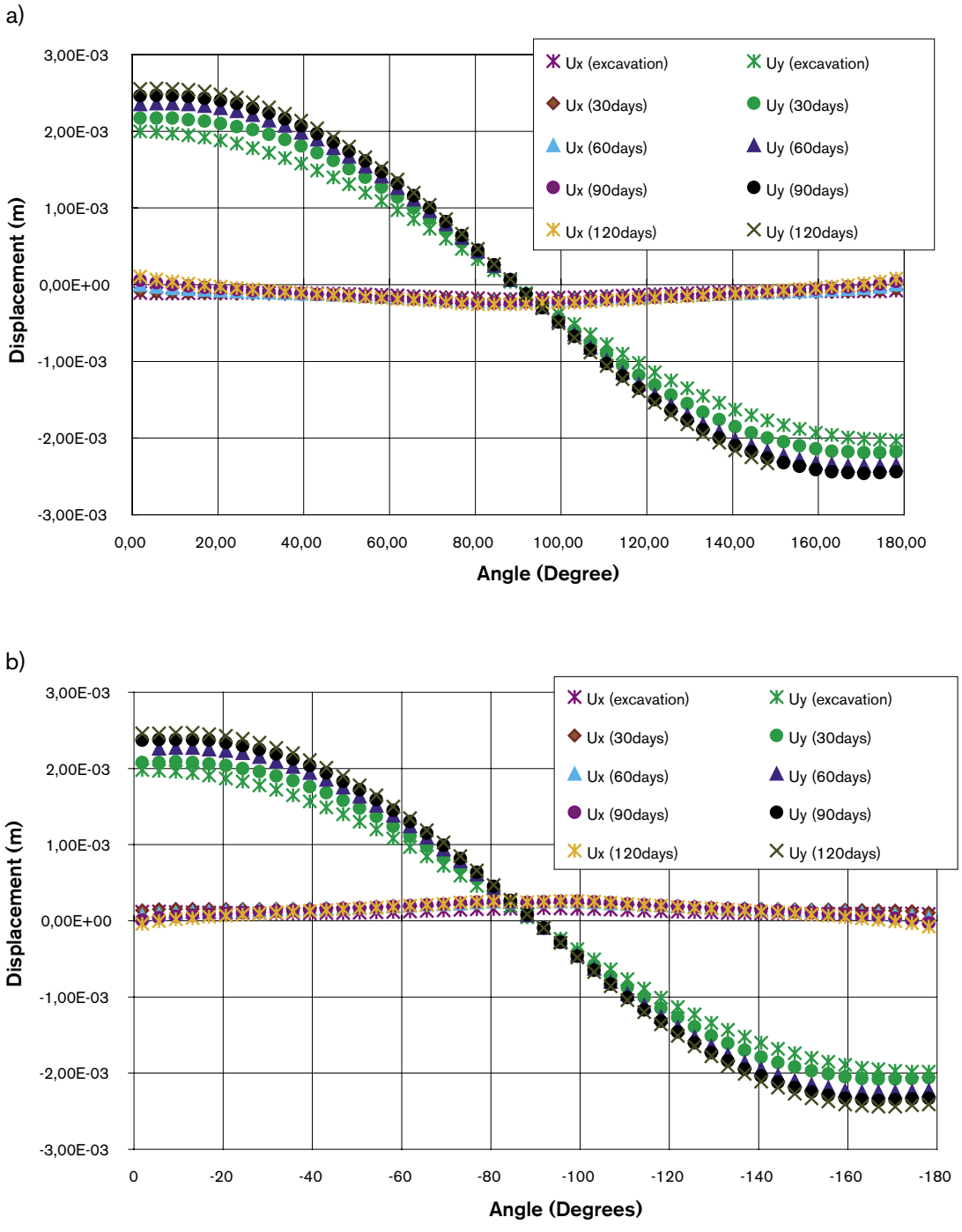


***Figure 6-5.*** *Displacement along pillar boundaries at 0.5 m section below the tunnel. (a) Left borehole wall. (b) Right confined borehole wall.*

### 6.1.3 Effect of pre-existing discontinuities

In Figure 2-4 a prediction of the discontinuities present in the pillar at 0.5 m depth are presented. The prediction is based on the mapping of the tunnel and the core boreholes in the vicinity of the pillar. Two different models where run. The first one only included the two sub-vertical NW trending fractures that cuts through the two holes closed to the pillar. These fractures where found to give a very limited impact on the stress field and the fracture propagation in the pillar. The second model included the shear-zone. The model studied the contacts presented in the figure so the rock between the two contacts was modelled with the same parameters as the rest of the rock in the pillar. The result is presented in Figure 6-6. The model predicts that some yielding will take place along the contacts and that the displacements will redistribute the stress field significantly. The changed stress field will result in a quite decreased fracture propagation compared to the intact pillar model.

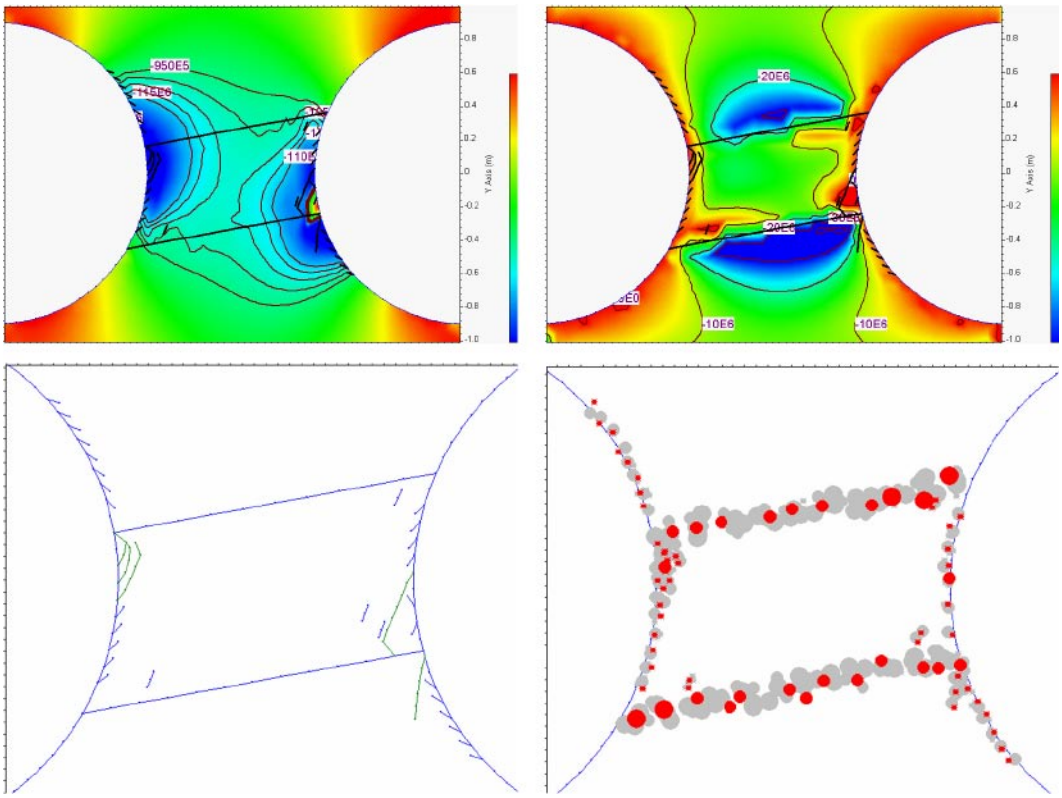


***Figure 6-6.*** *Effect of the shear-zone on the fracture propagation in the pillar after 120 days of heating. a) resulting fracture pattern. b) modelled AE. c) $\sigma_1$ distribution. d) $\sigma_3$ distribution.*

### 6.1.4 Spalling predicitons

*1. What is the failure criterion for spalling, i.e. where does one obtain it?*

In FRACOD the spalling is simulated by three processes; fracture initiation, failure of potential fracture planes and by fracture propagation. The criteria used in FRACOD to detect fracture initiation has been described thoroughly in /Rinne et al. 2003, Part II, Section 2.3/. Fracture initiation often starts from microcrack formation at a stress level of 0.3–0.6 of the rock strength. In this study we assume that when the stress reaches 50% of the rock strength at a given location, a potential macrocrack or a failure plane may form.

This discontinuity, however, has the intact rock strength. Local failure may take place and the fracture may propagate only when the strength of this surface is exceeded during the subsequent increase in stress. For this reason the level for fracture initiation is not critical for the final failure.

Tensile strength criterion is used in the direction perpendicular to the tensile stress. For shear fracture initiation, the Mohr-Coulomb failure criterion is used. Fracture initiation at boundaries of the boreholes as well as from the intact rock is considered.

Fracture propagation is modelled by the F-criterion. According to the F-criterion, in an arbitrary direction (θ) at a fracture tip there exists a F-value, which is calculated by

$$F(\theta) = \frac{G_I(\theta)}{G_{Ic}} + \frac{G_{II}(\theta)}{G_{IIc}}$$

where GIc and GIIc are the critical strain energy release rates for mode I and mode II fracture propagation; GI(θ) and GII(θ) are strain energy release rates due to the potential mode I and mode II fracture growth of a unit length. The direction of fracture propagation will be the direction where F reaches the maximum value. If the maximum F reaches 1.0, fracture propagation will occur.

*2. What is the tangential stress required to initiate spalling?*

Theoretically, applied parameters (cohesion c=31 MPa and intact rock friction φ=49° angle) gives a uni-axial strength of 166 MPa. FRACOD calculations suggest fracture initiation to start from the borehole boundary in the narrowest section of the pillar, when the tangential stresses reach a value of about 80 MPa (/Rinne et al. 2003/, Part I, Figure 4-3). Following the stress increase, the initiation will progress along the borehole wall.

FRACOD APSE models suggest fracture failure and fracture propagation when the maximum tangential stress exceeds 130 MPa. There are two reasons why the slippage (failure) of new fractures takes place before 166 MPa, as suggested by Mohr-Coulomb criterion. If the fracture stiffness of a new fracture is very high, the code would not feel its existence. If the stiffness is not that high, as in our case, there will be an additional deformation so the new fracture is felt as a defect. The stress redistributes around it and cause lower normal stress and higher shear stress. In addition, if there is more than one new fracture generated at once, the fractures affect each other and may result in early fracture slippage.

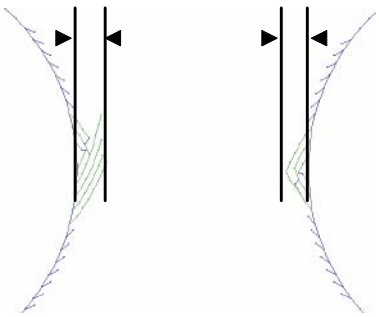

***Figure 6-7.*** *Depth of spalling in defined perpendicular from the tangent of the narrowest section of the pillar (horizontal section). Results are presented in Table 6-1.*

*3. How deep will spalling propagate as a function of stress, i.e. depth of failure.*

**Table 6-1. Depth of spalling as a function of stresses for each loading step.**

| Section | Excavation | 30 days | 60 days | 90 days | 120 days |
|---|---|---|---|---|---|
| **Section 1.5 m below tunnel floor** | | | | | |
| Maximum compressive stress (elastic model) | 122.5 MPa | 145.3 MPa | 161.7 MPa | 169.5 MPa | 175.8 MPa |
| Left borehole boundary | No fracture propagation | 0.11 m | 0.13 m | 0.13 m | 0.13 m |
| Right borehole boundary | No fracture propagation | 0.10 m | 0.12 m | 0.12 m | 0.12 m |
| **Section 0.5 m below tunnel floor** | | | | | |
| Maximum compressive stress (elastic model) | 140.2 MPa | 162.8 MPa | 179.3 MPa | 187.1 MPa | 193.4 MPa |
| Left borehole boundary | 0.11 m | 0.13 m | 0.13 m | 0.15 m | 0.15 m |
| Right borehole boundary | 0.04 m | 0.10 m | 0.12 m | 0.13 m | 0.13 m |

*4. The effect of confining stress on 1, 2 and 3.*

The confining stress for fracture initiation is taken into account in the Mohr-Coulomb failure criterion. The confinement for fracture propagation is considered by calculating the critical strain energy release rate for both mode I and mode II failure in varying directions.

The maximum compressive stress decrease and the confinement increases from the borehole boundary toward the pillar central. Level of confinement where the fracture propagation starts is less than $\sigma 3 < 5$ MPa and the fractures will not propagate inside the region where confinement is higher than $\sigma 3 > 20$ MPa (see Figure 3-2. in /Rinne et al. 2004/).

The modelled effect of confining pressure from hydraulic pressurisation has been reported in /Rinne et al. 2004/.

## 6.2 FLAC3D

FLAC3D is the only numerical code used in this project that performed coupled 3D thermal-mechanical predictions. The entire sequence with stress increases due to the excavations and thermal load is modelled with the same code. The results presented in this section are from /Wanne et al. 2004/.

### 6.2.1 Thermal predicitions

Adiabatic (fully insulated) boundaries have been used in the model. During the heating phase the floor of the experiment area will be insulated and the open hole will be covered to make the reality as close to the model as possible. The effect on the heaters is 200 W/m for all of the realisations of the model.

In Figure 6-8 the temperature in the centre of the pillar and the surrounding rock mass after 120 days of heating is presented. The temperature in the centre of the pillar is predicted to 60 to 65 degrees C and the highest temperature 65 to 70 degrees C is achieved between the two heaters at each side of the pillar.

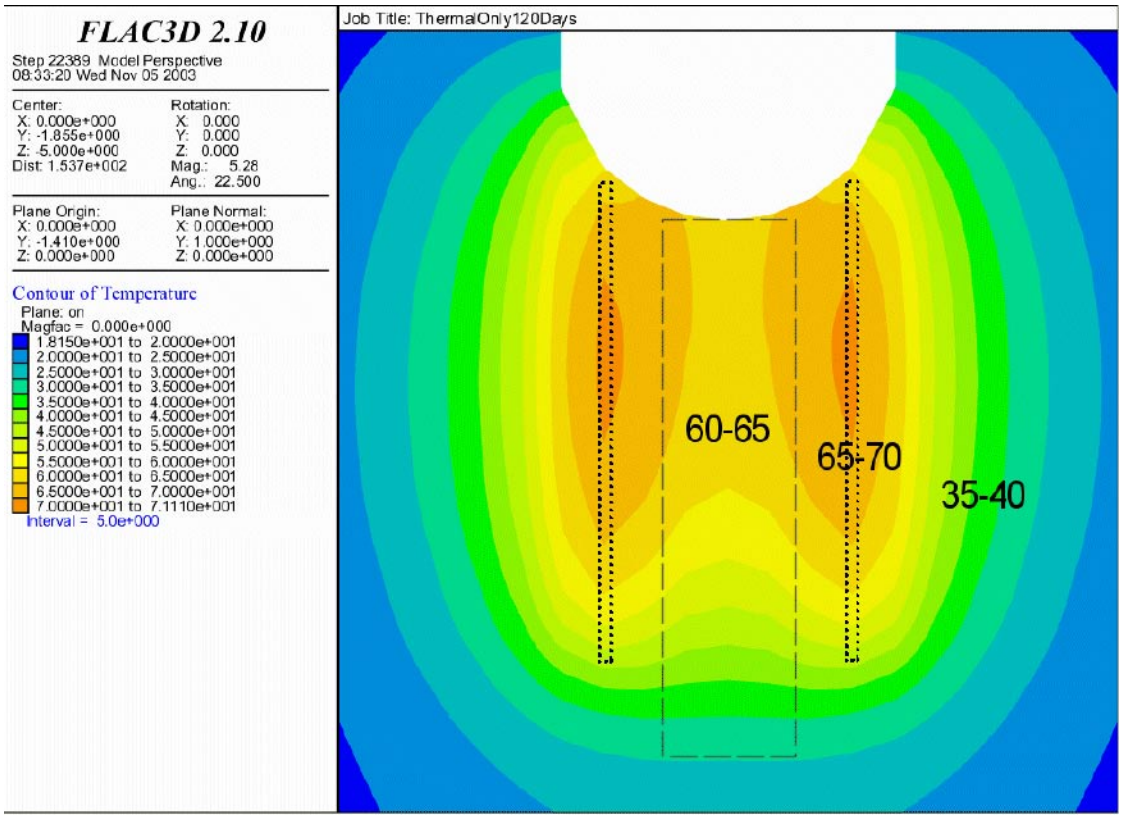


***Figure 6-8.*** *Temperature distribution in a vertical section cutting through the centre of the pillar after 120 days of heating. Dotted lines indicates the heater locations and the dashed line the deposition holes.*

The temperature development has been modelled between the two heaters on each side of the pillar and along the pillar wall in both deposition holes. An example of one temperature profile is presented in Figure 6-9. The graph presents the temperature development along the pillar wall in the open hole at four different depths. It takes approximately four days for the heat front to reach the centre of the pillar after the heaters are turned on.

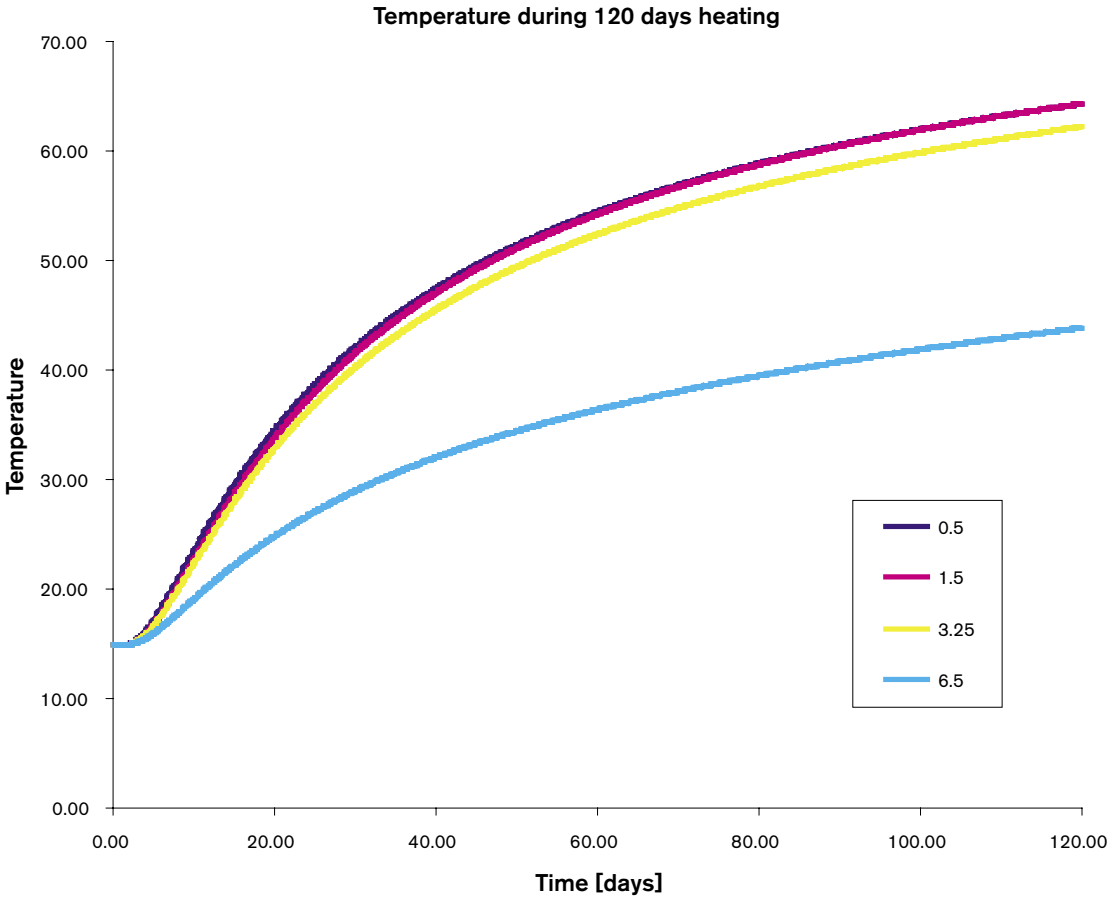


***Figure 6-9.*** *Temperature development at four different depths along the hole wall of deposition hole DQ0063G01 facing the pillar. Temperatures in degrees C.*

### 6.2.2 Predicted stresses

The FLAC3D model predicts a thermal contribution to the total stress at the hole wall of approximately 50 MPa at the 0.5 m level after 120 days of heating. Stress development over time for both the 0.5 and the 1.5 m level is presented in Figure 6-10. The parts of the pillar at both depths that are stressed over the crack initiation stress are illustrated in Figure 6-11. As can be seen in the figure the stresses at the 0.5 m level are over the crack initiation stress of 121 MPa throughout the pillar but only a limited part of the pillar area at 1.5 m depth is over the same threshold.

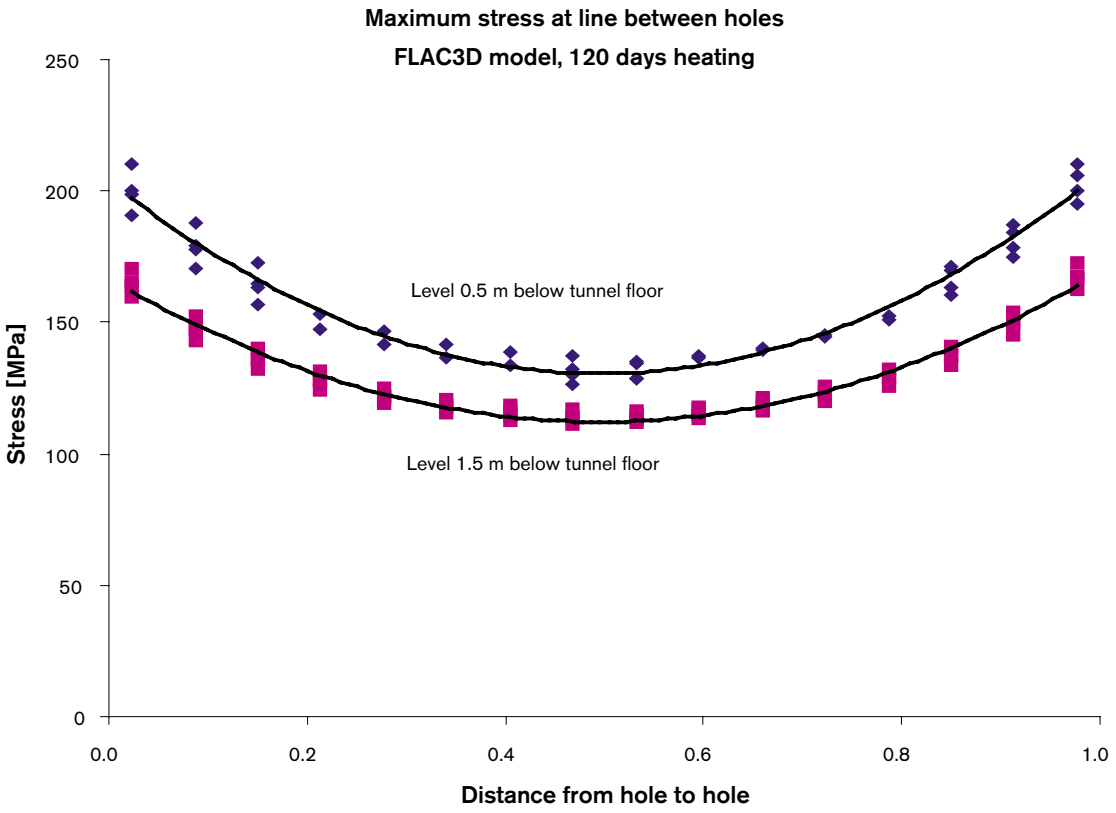


***Figure 6-10.*** *Maximum compressive stresses along lines between the deposition holes at the two depths of interest. The open hole wall is at X=0.0 and the confined hole wall at X=1.0.*

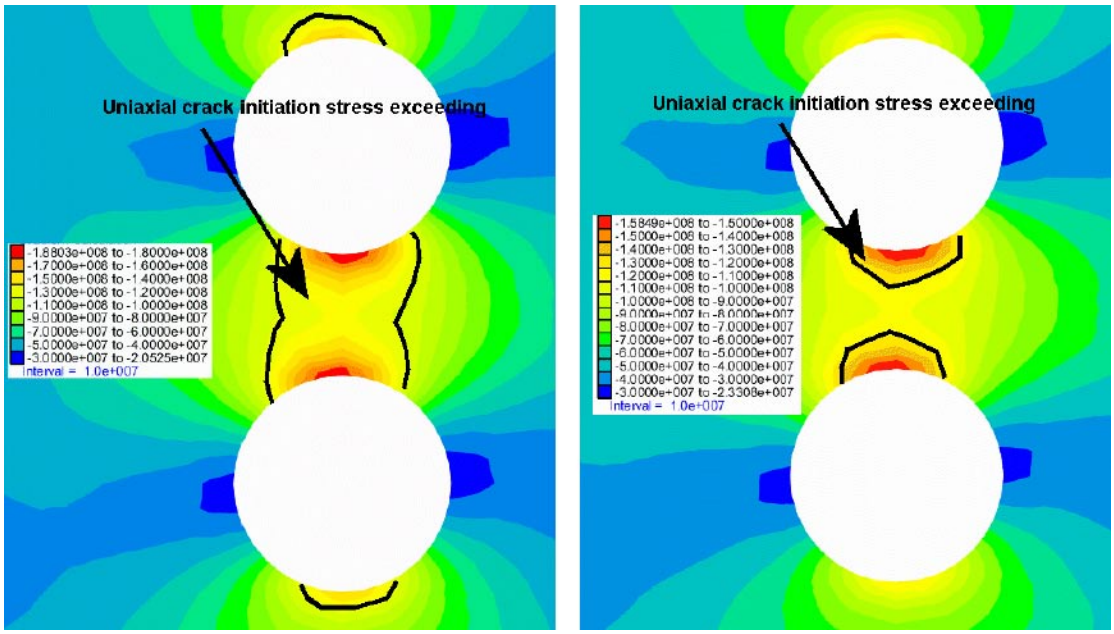


***Figure 6-11.*** *Areas with crack initiation stress exceedings at the 0.5 (left) and 1.5 m(right) levels after 120 days of heating.*

### 6.2.3 Displacements

FLAC3D results in similar displacement magnitudes, 1–2 mm, as the FRACOD-model. The resulting FLAC3D horizontal displacements after 120 days of heating are presented in Figure 6-12.

The 3D-model is also able to present the displacements as vectors. These results indicates that the pillar heaves approximately 1.5 mm at the top and as can be seen in Figure 6-13 the displacement vectors are directed quite steeply upwards. Figure 6-14 presents contributions from deformation after excavations and the deformation due to the heating of the rock. The displacements are given as the length of the vector.

Along the pillar wall the displacements that take place before the heating starts are almost negligible and are still very small after 120 days of heating. Comparing Figure 6-12 and Figure 6-14 makes it quite clear that the deformations along the pillar wall are almost only vertical.

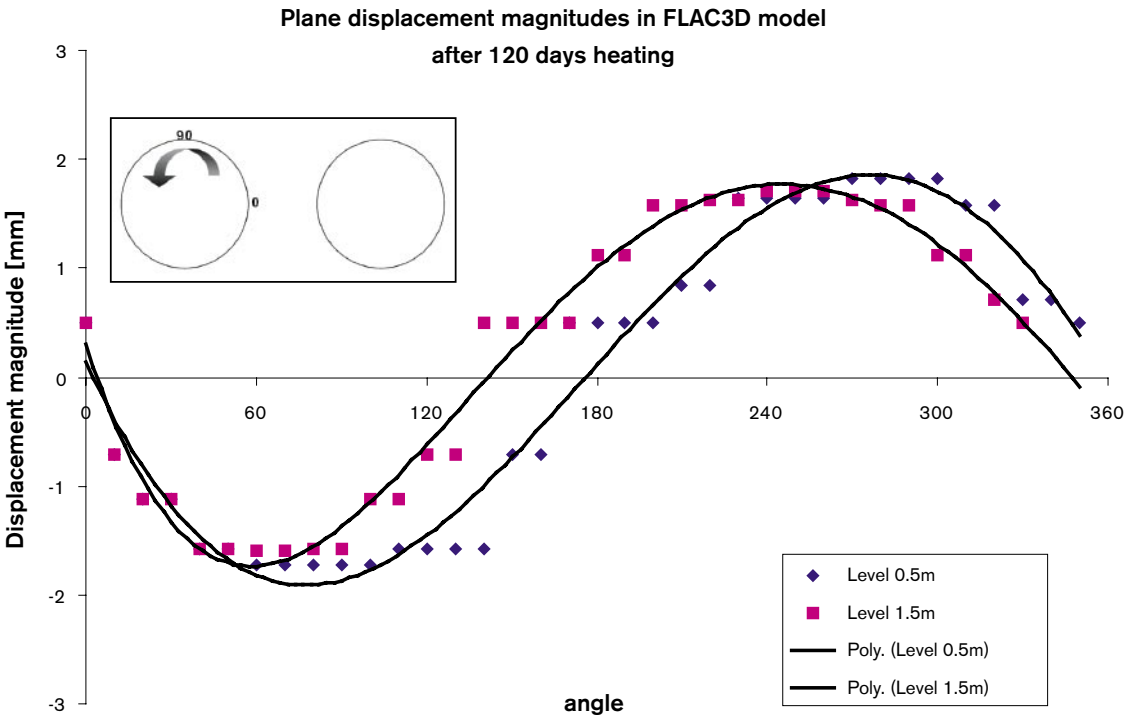


***Figure 6-12.*** *Displacement magnitudes at the hole wall 0.5 and 1.5 m below the tunnel floor. The displacement curve "hase shift" may be due inaccuracy in measurements. The accuracy of these displacement results is 0.5 mm.*

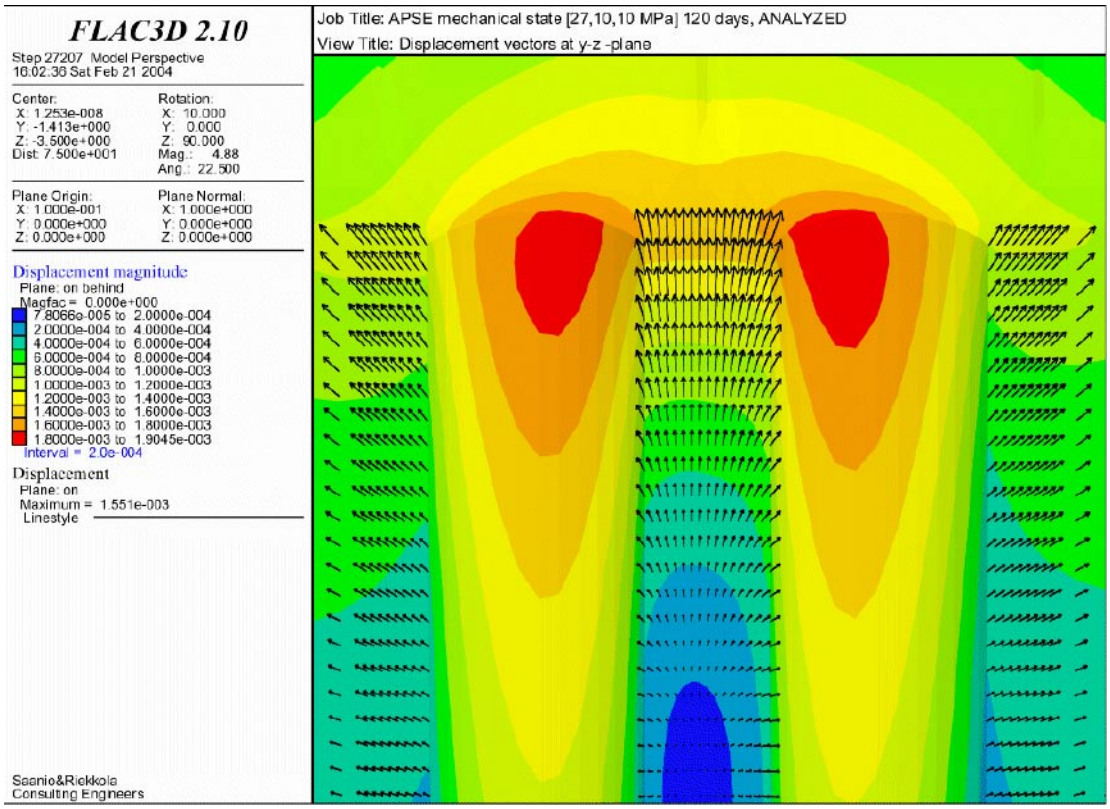


***Figure 6-13.*** *Resulting total displacement vectors and magnitude contour after 120 days of heating along a plane parallel to the tunnel-axis.*

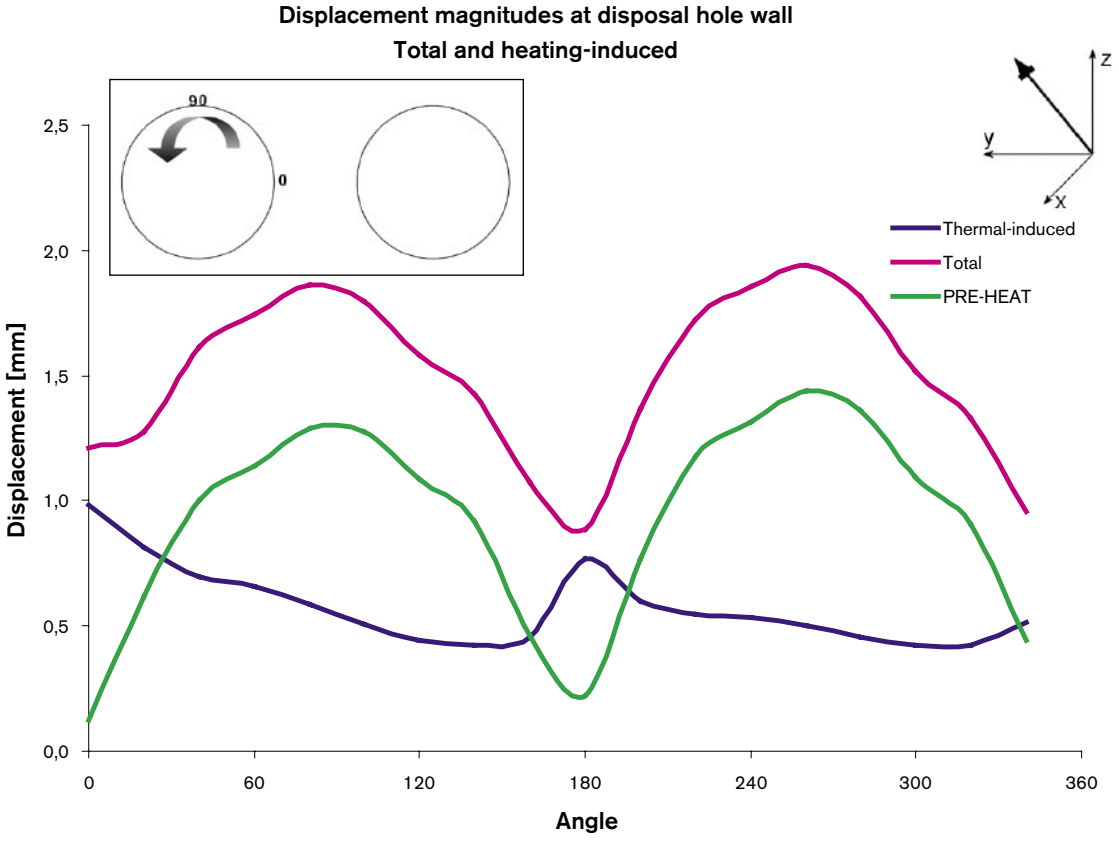


***Figure 6-14.*** *Displacement vector magnitudes at the hole wall 0.5 m below the tunnel floor. Total displacement is the sum of pre-heat and thermal-induced displacements. The displacements at the 1.5 m level are only a little smaller.*

### 6.2.4 Spalling predictions

*1. What is the failure criterion for spalling, i.e. where does one obtain it?*

Failure envelopes were composed assuming simplified linear relationship in σ1–σ3 space using the uni- and triaxial lab tests conducted by HUT. In addition, the following assumptions were used a) the crack initiation stress at $\sigma_3$=0 was fixed and given by SKB to be 121 MPa and b) the gradient for $\sigma_{ci}$ was assumed to be similar than for peak strength (although the gradient is much lower based on lab tests, see Figure 6-15). The composed stress-strength envelope is shown in Figure 6-15. (Figure 3-19 in /Wanne, 2004/). In the FLAC3D model only areas where $\sigma_{ci}$ exceeded were identified (see Figure 3-20 in /Wanne, 2004/).

*2. What is the tangential stress required to initiate spalling?*

Based on above the tangential stress at hole wall to initiate damage is 121 MPa at $\sigma_3$=0 (see note in item 3 on stresses at hole wall).

*3. How deep will spalling propagate as a function of stress, i.e. depth of failure.*

The damage areas extent about 1.7 m down to the hole. The depth of the damaged area is about 0.25 m and the width about 0.8 m on the top and 0.08 m and 0.4 m at the tip, respectively. It should be noted that the estimation of the damage area is controlled over the model element size in the pillar, which is about 5×15×25 cm (Figure 3-20 in the report). It should be also noted that the calculated stresses are average values in the center of a zone thus not giving the correct value at the hole wall. This slightly underestimates the damage area.

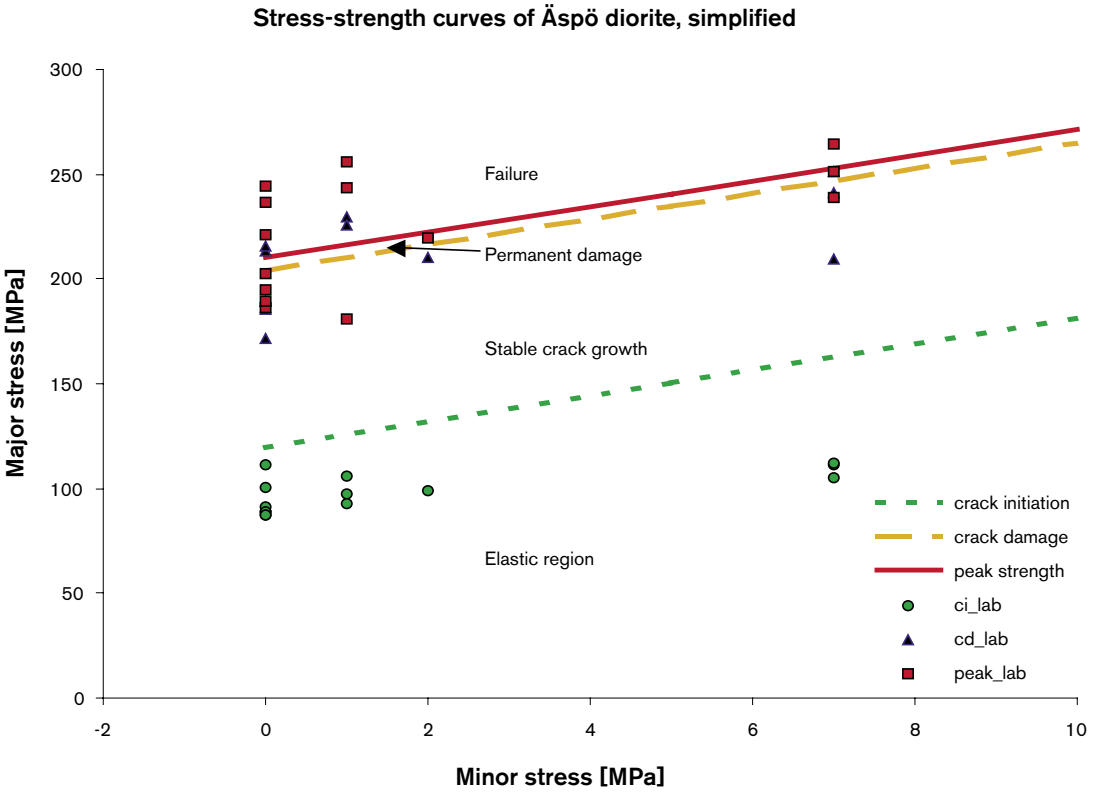


***Figure 6-15.*** *Failure envelope used in the analyses in the final report.*

*4. The effect of confining stress on 1, 2 and 3.*

All the above are based on the triaxial situation. The confining stress has a clear effect on the damage areas as shown in Figure 3-17 in the report. The failure envelope Figure 6-15 indicates that e.g. when confining pressure (minor stress) increases from 0 to 0.8 MPa the crack initiation stress increases by about 4% (121 to 125 MPa).

## 6.3 PFC2D

A coupled PFC2D-FLAC model has been used for some additional stress modelling of the 0.5 m level. The PFC model was 6.4 by 3.6 m consisting of 65,000 particles with an average diameter of 22 mm.

The PFC-model predicts fracturing of the hole walls (Figure 6-16) but to a less extent than what the others models predict.

Wanne et al. discuss the scale effect on the modelling and its impact on the results. The effect is not very well studied yet and it is therefore not known how the variability of the rock properties in a model like the APSE model shall be handled. An example of the impact of changes in the total stress or lowering of the rock strength is presented in Figure 6-17.

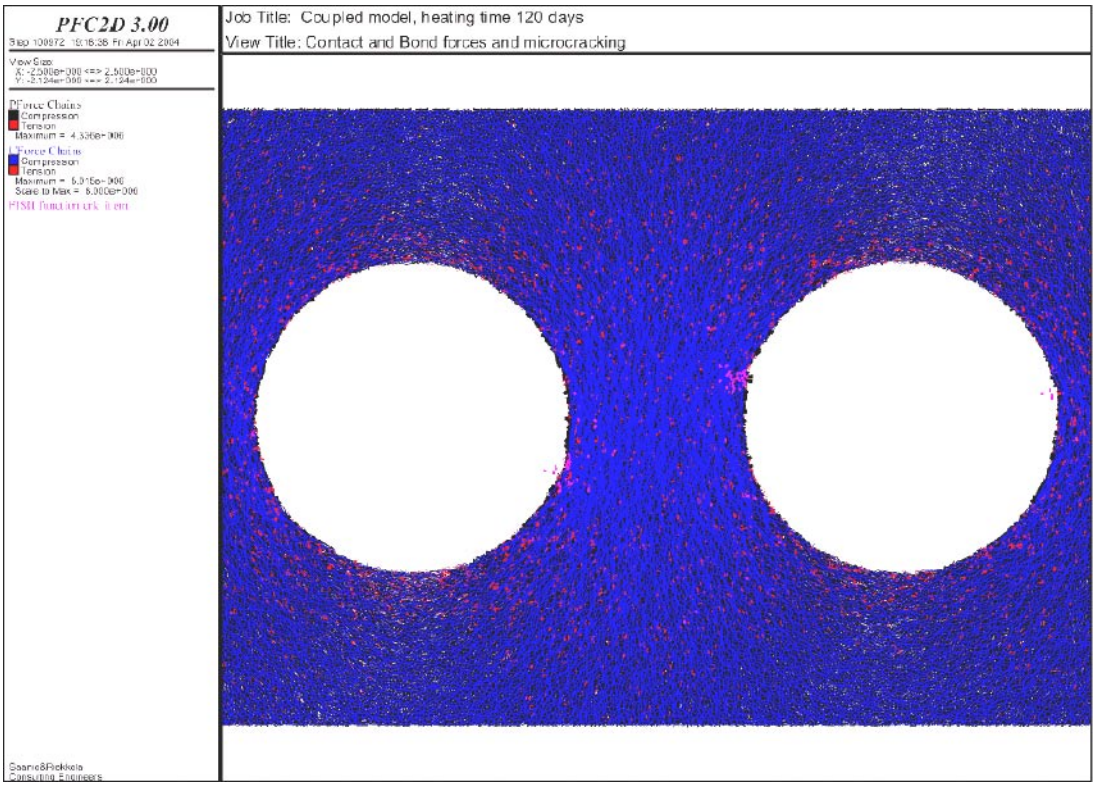


***Figure 6-16.*** *Forces and moment distribution and broken bonds (in magenta) after 120 days of heating. Blue is particle-particle compression, black and red are compression and tension in bond between particles.*

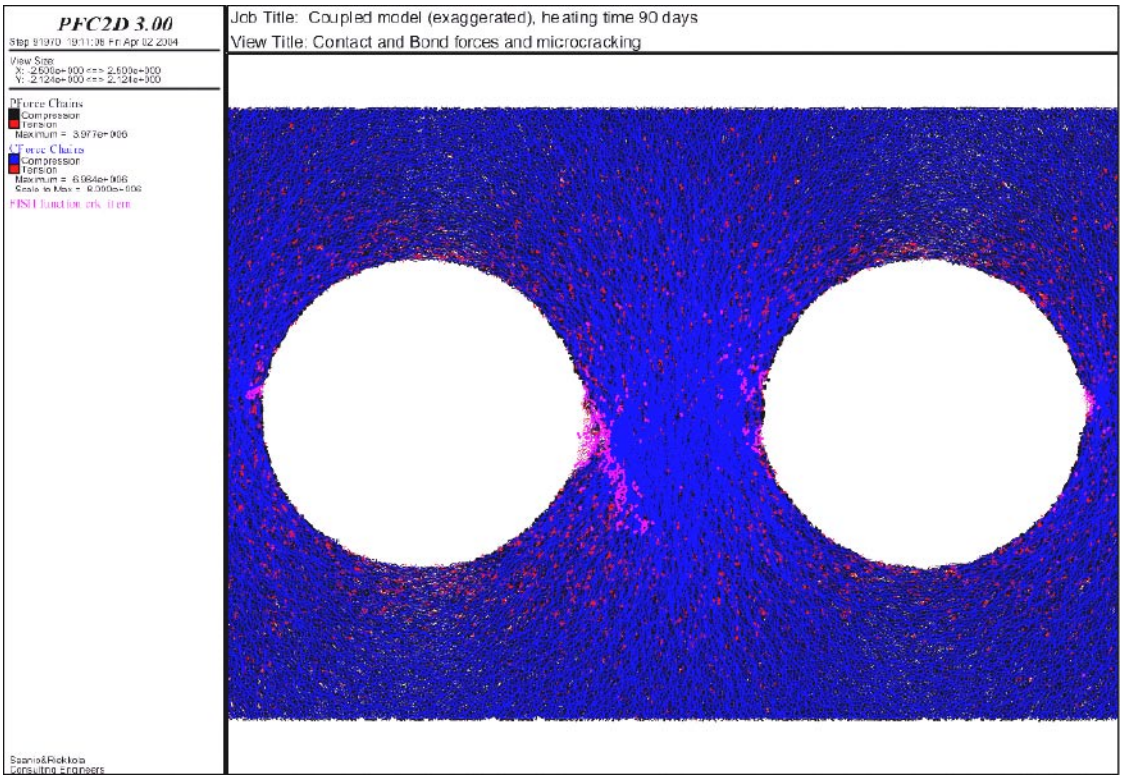


***Figure 6-17.*** *Damages at pillar when strength-reduction factor was 0.6. Forces and moment distribution and broken bonds (in magenta). Blue is particle-particle compression, black and red are compression and tension in bond between particles. Number of microcracks 304.*

## 6.4 JobFem

As earlier described 3D-stresses from Examine3D were transformed to 2D stresses in each node point of the finite element grid. The JobFem-code then applied temperature induced stresses to get the total stress field. In the early phase of the project the code was used for the design of the heaters including their geometrical placement and the effect they should have. Since the code is two dimensional the temperature predictions will be identical at the two levels of interest. All the results in this section is from Fredriksson et al. 2004.

### 6.4.1 Thermal predictions

In Figure 6-18 the temperature development in the pillar during the 120 days of heating is presented. The temperature is derived in a line going from the open hole to the confined one. There are slightly lower temperatures in the confined hole because of the approximately 12 $m^3$ water volume that's applying the confinement pressure in it.

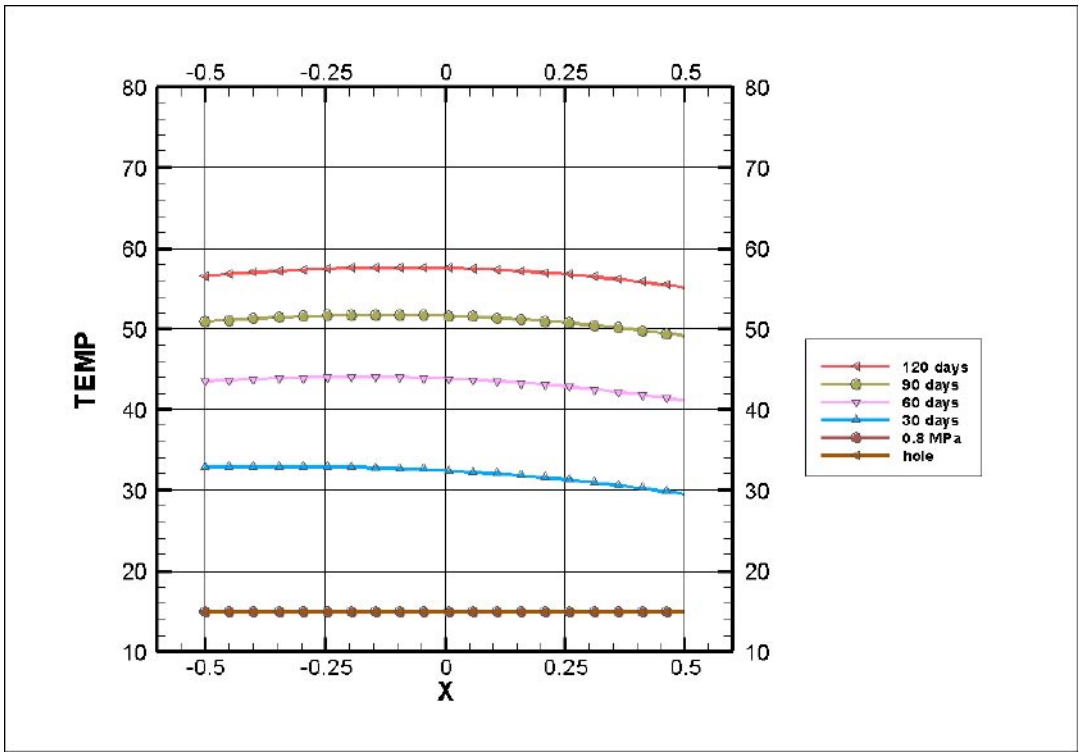


***Figure 6-18.*** *Temperature development in the pillar during the heating phase. X=–0.5 at the rim of the open hole and X=0.5 at the rim of the confined hole. The predictions are identical for the depth levels 0.5 m and 1.5 m.*

### 6.4.2 Predicted stresses

In Figure 6-19 and Figure 6-20 the predicted total major stress during the heating phase is presented for the 0.5 m and 1.5 m levels. In the figures the crack initiation stress (CIS) and the crack damage stress (CDS) are included as horizontal lines.

The total major stress at the 0.5 m level will be above the CIS throughout the pillar after approximately 60 days of heating. At the 1.5 m level the stress will only be above the CIS the 25 cm of rock that is closest to the hole walls. Approximately half the pillar area is hence below the crack initiation stress at this level.

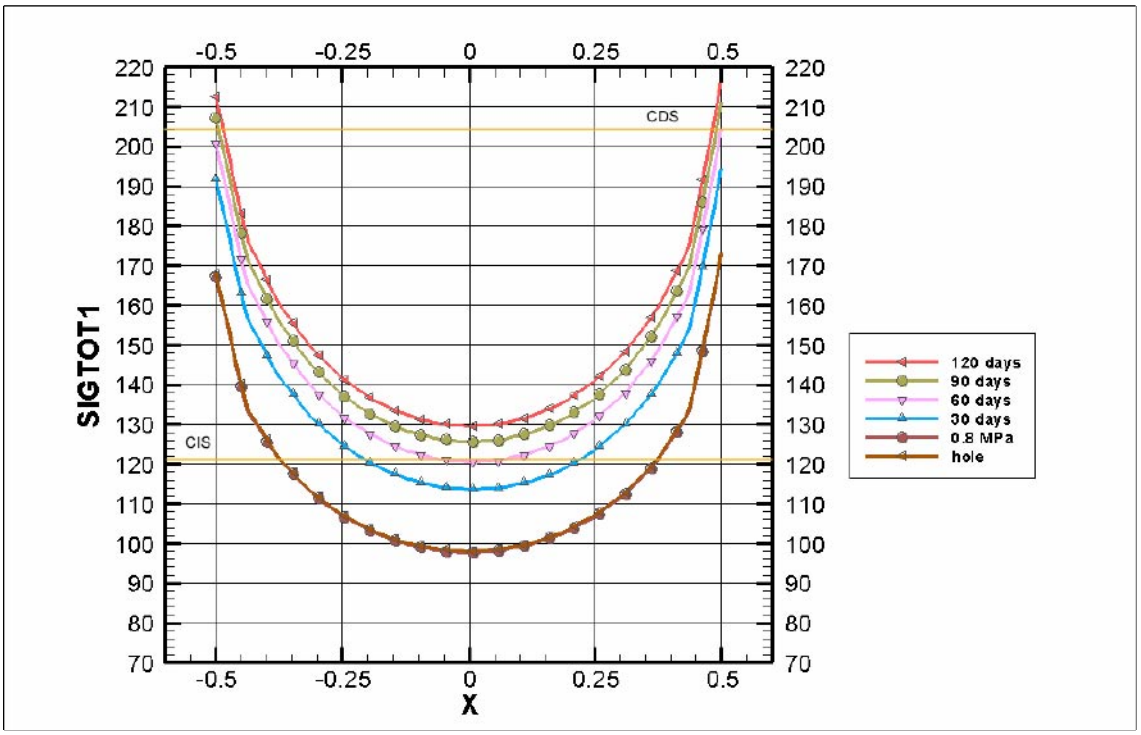


***Figure 6-19.*** *Total major stress throughout the pillar during the heating phase at the 0.5 m level. The open hole at X=–0.5 and the confined one at X=0.5*

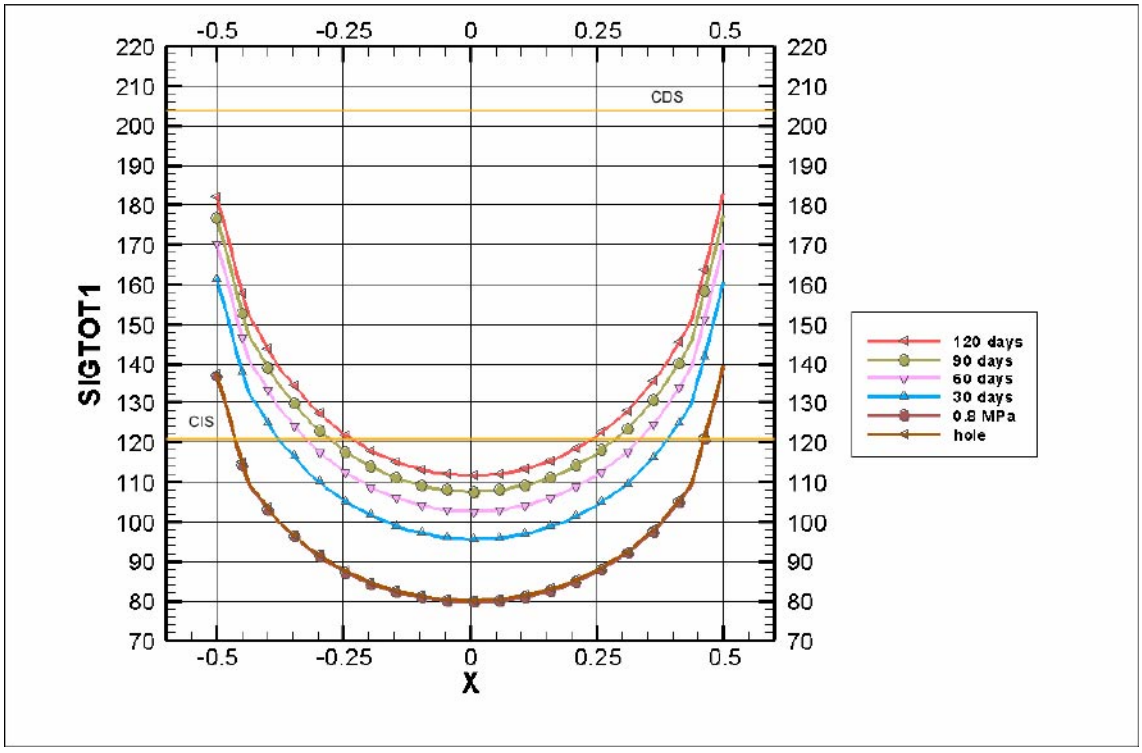


***Figure 6-20.*** *Total major stress throughout the pillar during the heating phase at the 1.5 m level. The open hole at X=–0.5 and the confined one at X=0.5*

### 6.4.3 Displacements

As for the other models the predicted displacements are quite small. Because of the fact that only stresses and not displacements were imported from Exmine3D the displacements that can be presented are only originating from the temperature increase. For the same reason the displacements at the two levels will become identical.

Figure 6-21 presents the vector deformations of the experiment area after approximately 30 days of heating. The deformations of the boarders of the open and confined hole throughout the heating phase are presented in Figure 6-22. The angles in Figure 6-21 correspond to the angles in Figure 6-22 and gives the location in each hole from where the actual displacement is derived.

The total displacements at the parts of the holes that faces the pillar is approximately 0.25 mm after 120 days of heating. The largest displacement will occur parallel to the direction of the major principal stress (at 0 and 180 degrees) and are modelled to approximately 0.5 mm.

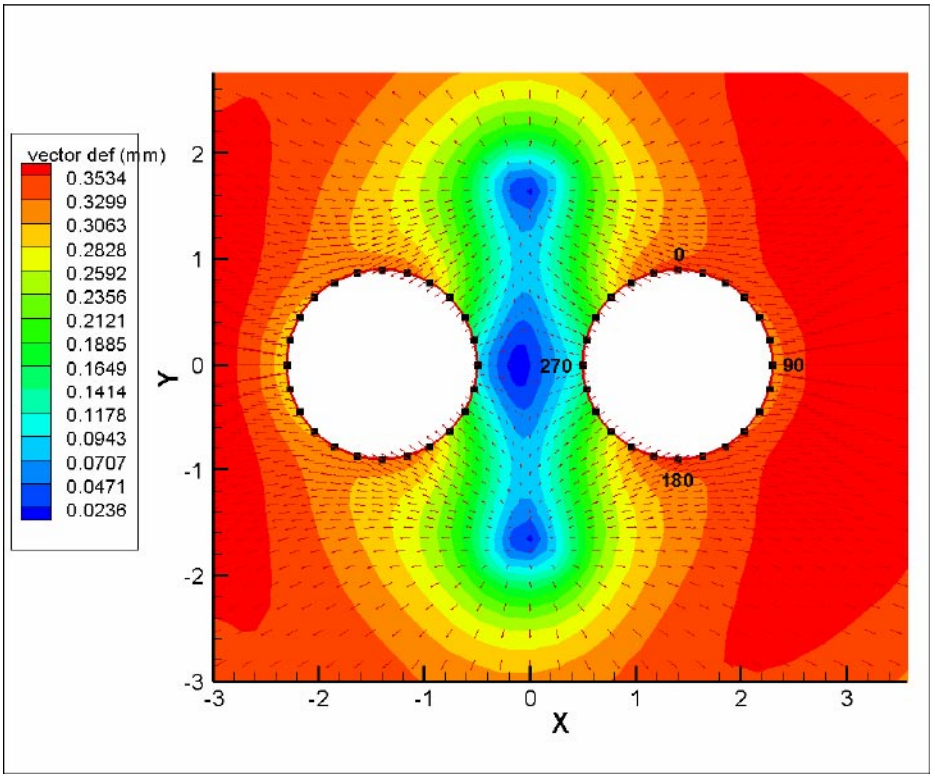


***Figure 6-21.*** *Vector deformations after approximately 30 days of heating.*

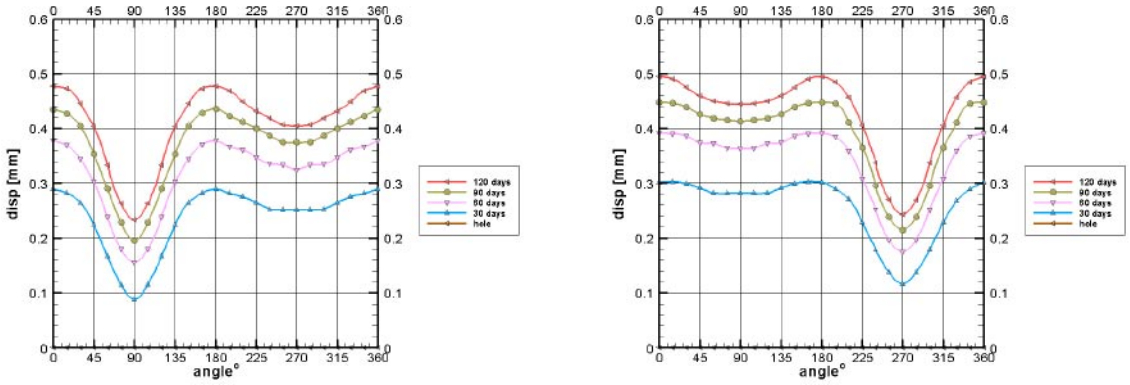


***Figure 6-22.*** *Vector displacements at the hole boundaries. a) open hole. b) confined hole.*

### 6.4.4 Spalling predictions

*1. What is the failure criterion for spalling, i.e. where does one obtain it?*

The spalling can be expected to take place where the difference between the major stress and the minor stress is greater than the Crack Initiation Stress (CIS).

*2. What is the tangential stress required to initiate spalling?*

See above.

*3. How deep will spalling propagate as a function of stress, i.e. depth of failure.*

The depths of penetration in the rock of the spalling zones are shown in. After 120 days of heating the spalling zone will have a depth of 0.20 m at 0.5 m below the tunnel floor and 0.12 m at 1.5 m below the tunnel floor.

**Table 6-2. Depth of penetration of the spalling zone.**

| | Depth of penetration of the spalling zone 0.5 m below the tunnel floor | Depth of penetration of the spalling zone 1.5 m below the tunnel floor |
|---|---|---|
| After axcavation | 0.07 m | 0.03 m |
| After 30 days of heating | 0.13 m | 0.06 m |
| After 60 days of heating | 0.16 m | 0.09 m |
| After 90 days of heating | 0.19 m | 0.10 m |
| After 120 days of heating | 0.20 m | 0.12 m |

*4. The effect of confining stress on 1, 2 and 3.*

The effect of confining stress has not been discussed in the report.

# 7 Discussion

Mainly the results from the FLAC3D and the JobFem codes will be discussed in this section as the results from the 3 and 2-dimensional models will be compared. The FRACOD model will be discussed on the basis of its sensitivity to input parameters.

## 7.1 2D and 3D continuum-models

The Äspö Pillar Stability Experiment has a complex geometry that required the use of both 2D and 3D numerical models. As been described earlier 3-dimensional stresses have been transformed to 2-dimensional when 2D-models have been used. These stresses were then used as a basic stress field in the modelled plane to which the thermal components were added. One could say that 2D-models are less efficient than 3-dimensional since a number of different actions have to be taken before the results can be produced in a problem like the APSE modelling but this is not completely true. In this case the 3D-stresses were derived with Examine3D which is fast and simple to operate. After a realisation the program gives the stress tensors at pre-selected co-ordinates in a separate result file. The transformation to 2D stresses is almost fully automated and therefore fast. The major advantage with 2D-models is that the building time for the model is much lower than for 3D models. This gives the possibility to quickly see how changes in geometries effect the final outcome of a prediction. On the other hand, the results from a 3D-model gives a much more complete understanding of the modelled volume since data of interest can be extracted from almost any point the model. If numerical modelling of the rock mass should be an important part of the design of a larger underground facility the ideal would be to use 2D-modelling to scope where there potential problems might occur and if necessary do 3D-modelling of such areas.

As been stated in the objectives for the Äspö Pillar Stability Experiment a comparison of the two- and three-dimensional modelling capabilities is to be performed. In the sections below comparisons have been made on the prediction results from the models and the actual time the modelling has taken.

## 7.2 Comparison of predictions

Comparisons of temperature and stress are presented in Table 7-1 and Table 7-2 respectively. The stress and temperature results for the FRACOD-model are not included since they are the same as for the JobFem model.

**Table 7-1. Comparison of predicted temperature at the 1.5 m level on the open hole wall after 30, 60, 90 and 120 days of heating.**

| Heating time (days) | FLAC3D (°C) | JobFem (2D) (°C) |
|---|---|---|
| 30 | 42 | 33 |
| 60 | 55 | 44 |
| 90 | 61 | 51 |
| 120 | 65 | 57 |

**Table 7-2. Comparison of predicted horizontal stresses on the hole wall and in the centre of the pillar after 120 days of heating.**

| | Hole wall 0.5 m level | Hole wall 1.5 m level | Pillar centre 0.5 m level | Pillar centre 1.5 m level |
|---|---|---|---|---|
| FLAC3D (MPa) | 200 | 162 | 130 | 112 |
| JobFem (D) (MPa) | 214 | 182 | 130 | 112 |

The resulting stress from FLAC3D and JobFem is almost identical but JobFem gives lower temperatures throughout the heating phase. The stresses end up the same despite the temperature difference since the stresses that were imported from Examine3D are approximately 15 to 20 MPa higher than the ones derived by FLAC3D. The difference between Examine3D and FLAC3D probably depends on that slightly different geometries have been used.

The three models, FRACOD, JobFem and FLAC3D give very similar displacements. During the heating phase the elastic horizontal displacement of the pillar wall is approximately 0.15 mm.

### 7.2.1 Spalling depth

The predicted spalling depths for the 2-dimensional codes are quite similar at the lower modelled level but differ 5 cm at 0.5 m depth. The 3D-code gives somewhat different results but as stated in the report the size of the elements in that model is quite large 5×15×25 cm. When predictions are made in small scale it is very important that the elements are small. The stresses will else be averaged over too large distances. The predicted depths for the different models after 120 days of heating are summarized in Table 7-3.

**Table 7-3. Predicted final spalling depths for the different models.**

| | JobFem2D | FRACOD2D | FLAC3D |
|---|---|---|---|
| Spalling depth 0.5 m (cm) | 20 | 15 | 25 |
| Spalling depth 1.5 m (cm) | 12 | 13 | 8 |

### 7.2.2 Effect of confining stress

According to the models the effect of the confinement will be quite small. In FRACOD a 10–20% reduction of fracture initiation and propagation is predicted in the confined hole. In FLAC the crack initiation stress is assessed to increase 4% due to the confinement. According to these results one should expect roughly the same amount of acoustic emission events and damage on both hole walls.

At the Underground Research Laboratory, URL, in Canada other findings have though been done. In both the Heated Failure Experiment and the Mine by Experiment /Read et al. 1997/ it was found that a small confining pressure gives clear effects on the spalling process. The APSE is designed to make a comparison with the URL-results possible and it will be very interesting to see the outcome.

## 7.3 Comparison of time used for modelling

For the building of the initial model it took approximately 5 times longer to build the FLAC3D model than building any of the 2D-models together with the Examine3D model together. The time for a correction of the geometrical model takes 10–20 times longer in FLAC3D. The calculation times needed for FLAC3D, FRACOD and JobFem are approximately the same.

It can be concluded that the difference in time between the 2D and 3D model building is from a few days to a few weeks. The time difference for making changes in the models is from a couple of hours to a couple of days for the 2D and 3D models respectively.

## 7.4 Modelling of fracture initiation and propagation

Fracture initiation and propagation is a difficult task to model. The rock mechanical properties with their spatial distribution and the detailed geological knowledge needed to be able to make accurate predictions will never be known for any practical application. The resulting fracture patterns from the FRACOD-model are therefore an indication of the extent of damage to the rock.

In the main FRACOD report the effect of pre-existing discontinuities has been modelled. The code is able to model the stability of the discontinuities and the stress re-distribution due to eventual yielding along them. If the behaviour of discontinuities is a concern and the problem can be modelled in 2D, FRACOD seems to be suitable but first the model's sensitivity to fracture stiffness and fracture toughness needs to be verified better. Quite extensive laboratory tests were performed on fracture stiffness and especially the results on the fracture normal stiffness are questionable. The standard deviation is of the same magnitude as the mean value giving a large range of probable values. As a part of the modelling sensitivity analyses were performed. The analysis compared the fracture initiation and propagation to results using averaged parameters. Relative comparisons were made and a subjective judgement of the effect of the changed parameter/parameters done. The analysis resulted in that changes in the stiffness had a very minor effect on the modelling results after a reaching a certain threshold.

The model sensitivity to the fracture toughness in mode I is small. For the mode II fracture stiffness the sensitivity is small above a threshold value. The methods for determining the stiffness and toughness are quite novel and as abovementioned the variation in the stiffness results was large. Since laboratory testing is expensive and time consuming it is important that the code's response to the input parameters is well understood. Currently it seems questionable to make efforts on extensive laboratory testing if threshold values, possibly easily assessed, can be used instead of mean values from laboratory testing.

# 8 References

**Andersson J C, Eng A.** Äspö Pillar Stability Experiment, Thermal and displacement monitoring. Instrument specifications and measured data report. SKB report R-05-02, Svensk Kärnbränslehantering AB.

**Andersson J C.** Äspö Pillar Stability Experiment, Feasibility Study. SKB report IPR-03-01, Svensk Kärnbränslehantering AB.

**Andersson J C, Martin C D.** Katsuhiko Sugawara, Yuozo Obara & Akira Sato and Katsuhiko Sugawara, Yuozo Obara & Akira Sato (ed.). Stress variability and the design of the Äspö Pillar Stability Experiment. In the proceedings of the third internation symposium on rock stress. RS Kumamoto '03, 4–6 November 2003, Kumamoto Japan, p. 321–326

**Fredriksson A, Staub I, Outters N.** Äspö Pillar Stability Experiment, Final 2D couple thermo-mechanical modelling. SKB report R-04-02, Svensk Kärnbränslehantering AB.

**Fredriksson A, Staub I, Janson T.** Äspö Pillar Stability Experiment, Design of heaters and preliminary results form coupled 2D thermo-mechanical modelling. SKB report IPR-03-03, Svensk Kärnbränslehantering AB.

**Read R S, Chandler N A.** An approach to excavation design for a nuclear fuel waste repository – The thermal-mechanical stability study, final report. Ontario Power Generation report no. 06819-REP-01200-10086-R00. Toronto Canada 2002.

**Rinne M, Shen B, Lee H-S.** Äspö Pillar Stability Experiment, Modelling of fracture stability by FRACOD. Preliminary results. SKB report IPR-03-05, Svensk Kärnbränslehantering AB.

**Rinne M, Lee H-S, Shen B.** Äspö Pillar Stability Experiment, Modelling of fracture stability by FRACOD. SKB report R-04-04, Stockholm Sweden

**Staub I, Andersson J C, Magnor B.** Äspö Pillar Stability Experiment, Geology and mechanical properties of the rock in TASQ. SKB report R-04-01, Svensk Kärnbränslehantering AB.

**Wanne T, Johansson E.** Äspö Pillar Stability Experiment, Coupled 3D thermo – mechanical modelling Preliminary results. SKB report IPR-03-04, Svensk Kärnbränslehantering AB.

**Wanne T, Johansson E, Potyondy D.** Äspö Pillar Stability Experiment, Final Coupled 3D thermo – mechanical modeling. Preliminary Particle – mechanical modeling. SKB report R-04-03, Svensk Kärnbränslehantering AB.